Remote Sensing of Environment 139 (2013) 231–245

Contents lists available at ScienceDirect

Remote Sensing of Environment

journal homepage: www.elsevier.com/locate/rse

High-resolution airborne hyperspectral and thermal imagery for early detection of *Verticillium* wilt of olive using fluorescence, temperature and narrow-band spectral indices

R. Calderón, J.A. Navas-Cortés, C. Lucena, P.J. Zarco-Tejada *

Instituto de Agricultura Sostenible (IAS), Consejo Superior de Investigaciones Científicas (CSIC), Córdoba, Spain

ARTICLE INFO

Article history:
Received 27 July 2012
Received in revised form 24 July 2013
Accepted 27 July 2013
Available online xxxx

Keywords:
Stress detection
Hyperspectral
Thermal
Fluorescence
High resolution
UAV
Physiological indices
Verticillium dahliae

ABSTRACT

Verticillium wilt (VW) caused by the soil-borne fungus *Verticillium dahliae* Kleb, is the most limiting disease in all traditional olive-growing regions worldwide. This pathogen colonizes the vascular system of plants, blocking water flow and eventually inducing water stress. The present study explored the use of high-resolution thermal imagery, chlorophyll fluorescence, structural and physiological indices (xanthophyll, chlorophyll a + b, carotenoids and blue/green/red B/G/R indices) calculated from multispectral and hyperspectral imagery as early indicators of water stress caused by VW infection and severity. The study was conducted in two olive orchards naturally infected with *V. dahliae*. Time series of airborne thermal, multispectral and hyperspectral imagery was acquired in three consecutive years and related to VW severity at the time of the flights. Concurrently to the airborne campaigns, field measurements conducted at leaf and tree-crown levels showed a significant increase in crown temperature (Tc) minus air temperature (Ta) and a decrease in leaf stomatal conductance (G) across VW severity levels, identifying VW-infected trees at early stages of the disease. Higher Tc − Ta and G values measured in the field were associated with higher VW severity levels. At leaf level, the reduction in G caused by VW infection was associated with a significant increase in the Photochemical Reflectance Index (PRI_{570}) and a decrease in chlorophyll fluorescence (F). The airborne flights enabled the early detection of VW by using canopy-level image-derived airborne Tc − Ta, Crop Water Stress Index (CWSI) calculated from the thermal imagery, blue/blue–green/blue–red ratios (B/BG/BR indices) and chlorophyll fluorescence, confirming the results obtained in the field. Airborne Tc − Ta showed rising values with a significant increase of ~2 K at low VW severity levels, and was significantly correlated with G ($R^2 = 0.76$, $P = 0.002$) and PRI_{570} ($R^2 = 0.51$, $P = 0.032$). Early stages of disease development could be differentiated based on a CWSI increase as VW developed, obtaining a strong correlation with G ($R^2 = 0.83$, $P < 0.001$). Likewise, the canopy-level chlorophyll fluorescence dropped at high VW severity levels, showing a significant increase as disease progressed. These results indicate the potentials of an early detection of *V. dahliae* infection and discrimination of VW severity levels using remote sensing. Indicators based on crown temperature such as CWSI, and visible ratios B/BG/BR as well as fluorescence were effective in detecting VW at early stages of disease development. In affected trees, the structural indices PRI, chlorophyll and carotenoid indices, and the R/G ratio were good indicators to assess the damage caused by the disease.

1. Introduction

Verticillium wilt (VW) of olive (*Olea europea* L.) trees, caused by the soil-borne fungus *Verticillium dahliae* Kleb., is the most limiting disease of this crop in all traditional olive-growing regions worldwide (Jiménez-Díaz et al., 2012; Tsror (Lahkim), 2011) and causes severe yield losses and tree mortality (Levin, Lavee, & Tsror, 2003). In Spain, the first reports of the disease, which was found to affect olive crops in the Guadalquivir valley, were documented in the early 1980s (Blanco-López, Jiménez-Díaz, & Caballero, 1984). However, in the last 15–20 years the disease has spread to affect newly established irrigated crops (Jiménez-Díaz, Olivares-García, Landa, Jiménez-Gasco, & Navas-Cortés, 2011; Sánchez-Hernández, Ruiz-Dávila, Pérez de Algaba, Blanco-López, & Trapero-Casas, 1998). Under field conditions, the first VW symptoms in irrigated olive trees growing in *V. dahliae*-infested orchards develop 18–24 months after plantation, depending on the density of pathogen propagules in the soil, the *V. dahliae* pathotype prevailing in the soil, the olive cultivar susceptibility and the environmental conditions (Levin et al., 2003; Navas-Cortés et al., 2008). In the

* Corresponding author at: Instituto de Agricultura Sostenible (IAS), Consejo Superior de Investigaciones Científicas (CSIC), Alameda del Obispo, s/n, 14004 Córdoba, Spain. Tel.: +34 957 499 280, +34 676 954 937; fax: +34 957 499 252.
E-mail address: pzarco@ias.csic.es (P.J. Zarco-Tejada).
URL: http://quantalab.ias.csic.es (P.J. Zarco-Tejada).

0034-4257/$ – see front matter
http://dx.doi.org/10.1016/j.rse.2013.07.031

Mediterranean region, over an annual cropping season, disease incidence and symptom severity typically increase from late autumn–early winter to spring and sharply decrease in summer, with no further development until the next autumn; this results in polyetic epidemics over several cropping seasons (Navas-Cortés et al., 2008).

V. dahliae can be found in agricultural soils as resistant survival structures called 'microsclerotia' that are stimulated to germinate by root exudates (Schreiber & Green, 1963) and favorable soil environmental conditions, forming hyphae that penetrate into the plant roots and grow into their tissues until they reach the xylem vessels. The rapid upward spread of the pathogen in vascular tissues occurs primarily through conidia transported with the transpiration stream (Emechebe, Leaky, & Banage, 1975; Garber & Houston, 1966; Presley, Carns, Taylor, & Schnathorst, 1966; Talboys, 1962). This enables the pathogen to spread throughout the aerial parts of its host within one growing season. The net effect of pathogen infection is a reduction in water flow that induces water stress and is thought to be mainly responsible for the vascular wilt syndrome caused by *V. dahliae* and other wilt pathogens (Ayres, 1978; DeVay, 1989; Van Alfen, 1989).

Water stress in plants caused by either *V. dahliae* infection or drought-induced stomatal closure reduces the transpiration rate. In turn, this decreases evaporative cooling and increases leaf temperature. Early detection of water stress using remote sensing has been successfully achieved in the past using thermal infrared radiation (Idso, Jackson, & Reginato, 1978; Idso, Jackson, Pinter, Reginato, & Hatfield, 1981; Jackson & Pinter, 1981; Jackson, Idso, Reginato, & Ehrler, 1977, Jackson, Idso, Reginato, & Pinter, 1981). Thermal remote sensing of water stress has been fulfilled using spectrometers at ground level (Idso et al., 1981, 1978; Jackson et al., 1977, 1981), thermal sensors at image level (Berni, Zarco-Tejada, Suárez, & Fereres, 2009; Cohen, Alchanatis, Meron, Saranga, & Tsipris, 2005; Leinonen & Jones, 2004; Sepulcre-Cantó et al., 2006, 2007; Zarco-Tejada, González-Dugo, & Berni, 2012) and satellite thermal imagery (Sepulcre-Cantó et al., 2009). Working with hand-held infrared thermometers on herbaceous crops, Jackson and co-workers (Idso et al., 1978; Jackson et al., 1981) developed the Crop Water Stress Index (CWSI), which became a popular thermal-based stress indicator. The CWSI is based on the normalization of differences between canopy (Tc) and air temperature (Ta) with evaporative demand (by means of the vapor pressure deficit). Apart from the progress made in water-stress detection using the thermal region, the visible part of the spectrum has also been useful for early water stress detection. This involves using indices focused on bands located at specific wavelengths where photosynthetic pigments are affected by stress conditions. Two spectral indicators of water stress, spanning initial through severe disease symptoms, are widely used. One is the Photochemical Reflectance Index (PRI) (Gamon, Peñuelas, & Field, 1992). This index is sensitive to the epoxidation state of the xanthophyll cycle pigments and to photosynthetic efficiency, serving as a proxy for water stress detection (Peguero-Pina, Morales, Flexas, Gil-Pelegrín, & Moya, 2008; Suárez, Zarco-Tejada, Berni, González-Dugo, & Fereres, 2009; Suárez et al., 2010; Suárez et al., 2008; Thenot, Méthy, & Winkel, 2002). Another indicator of water stress is solar-induced chlorophyll fluorescence emission (Flexas, Briantais, Cerovic, Medrano, & Moya, 2000, 1999, Flexas, Escalona, & Medrano, 1999, Flexas et al., 2002; Moya et al., 2004; Zarco-Tejada et al., 2009, 2012), because of the strong correlation found between steady-state chlorophyll fluorescence and the reduced assimilation caused by water stress conditions. The PRI has been used to assess pre-visual water stress at leaf level (Thenot et al., 2002; Winkel, Méthy, & Thénot, 2002), at canopy level (Dobrowsky, Pushnik, Zarco-Tejada, & Ustin, 2005; Evain, Flexas, & Moya, 2004; Peguero-Pina et al., 2008; Sun et al., 2008) and using airborne imaging spectroscopy (Suárez et al., 2009, 2010, 2008). Chlorophyll fluorescence is associated with photosynthesis and other physiological processes, as demonstrated consistently in laboratory studies (e.g., Krause & Weis, 1984; Papageorgiu, 1975). Over the last five years, scientific interest in steady-state chlorophyll fluorescence (Fs) obtained under natural outdoor conditions has increased due to its potential development using remote sensing methods (Soukupová et al., 2008). Although the contribution of fluorescence to the vegetation's radiance signal is estimated to be 2–3%, methods have been developed to extract the signal (Meroni, Colombo, & Cogliati, 2004; Meroni, Picchi, et al., 2008; Meroni, Rossini, et al., 2008; Meroni et al., 2009; Moya et al., 2004), proving the feasibility of the fluorescence retrieval using the O_2-A absorption feature at 760 nm.

Remote sensing has been used to detect, monitor and quantify a range of diseases in different crops. Comprehensive reviews on the application of remote sensing to the detection of plant diseases are available (e.g., Barton, 2012; Hatfield & Pinter, 1993; Jackson, 1986; Nilsson, 1995; Sankaran, Mishra, Ehsani, & Davis, 2010; West et al., 2003). Most studies have focused on foliar pathogens in annual crops, where disease symptoms are mainly characterized by distinct color changes in the aerial parts of the plant. However, this technology also has shown potential for detecting root diseases in several crops (e.g., Raikes & Burpee, 1998; Reynolds, Windels, MacRae, & Laguette, 2012; Wang, Kurle, Estevez de Jensen, & Percich, 2004). Canopy temperature has shown to be particularly useful to detect root impairment caused by soil-borne pathogens that lead to water stress symptoms, as mentioned above. In fact, Pinter et al. (1979) found foliar temperatures 3–4 °C higher than those of healthy plants in sugar beet and cotton. Other examples of the use of leaf temperature for the detection of diseases caused by soil-borne pathogens include beans infected with *Fusarium solani*, *Pythium ultimum* or *Rhizoctonia solani* (Tu & Tan, 1985); soybeans affected by brown stem rot caused by *Phialophora gregata* (Mengistu, Tachibana, Epstein, Bidne, & Hatfield, 1987); the flag leaf temperature of cereals with root and vascular diseases, such as barley infected by *Pyrenophora graminea* and wheat infected with *Cephalosporium gramineum* (Nilsson, 1995); and wheat with moderate take-all symptoms caused by *Gaeumannomyces graminis* var. *tritici* (Nilsson, 1991).

Other approaches have included the use of multispectral and hyperspectral imagery, as well as airborne digital color or video imagery, to detect crop diseases. Multispectral imagery enabled the detection of head blight in winter wheat (Dammer, Möller, Rodemann, & Heppner, 2011), assessment of severity of soybean root rot (Wang et al., 2004) and to evaluate *Rhizoctonia* blight in creeping bentgrass (Raikes & Burpee, 1998). Hyperspectral canopy reflectance was used to quantify *Rhizoctonia* crown and root rot in sugar beet (Reynolds et al., 2012) and to detect the co-infection of sugar beet with this pathogen and the plant parasitic nematode *Heterodera schachatii* (Hillnhütter, Mahlein, Sikora, & Oerke, 2011) as well as *Fusarium* head blight in wheat (Bauriegel, Giebel, Geyer, Schmidt, & Herppich, 2011).

Some research has been conducted on remote detection of diseases caused by *V. dahliae*. Nilsson (1995) reported that oilseed rape plants infected with *V. dahliae* exhibited leaf temperatures 5–8 °C higher than non-infected plants. Chen et al. (2008, 2011) reported the application of hyperspectral reflectance to identify cotton canopy affected by VW. They found that the spectral characteristics of infected plants changed gradually with the increase in the visible region with disease severity, while a reduction occurred in the near-infrared region. Yet, to our knowledge remote sensing physiological indices and fluorescence indicators have not been used to study olive tree diseases.

The main objective of this research was to evaluate the use of high-resolution thermal imagery and physiological indices calculated from multispectral and hyperspectral imagery as indicators of VW infection and severity in olive orchards. Time series of airborne thermal, multispectral and hyperspectral imagery were acquired in three consecutive campaigns and related to VW severity at the time of the flight. The hypothesis is that thermal and hyperspectral indices acquired from the airborne imagery are sensitive to physiological changes induced by the infection and colonization by *V. dahliae*.

2. Materials and methods

2.1. Study site description

The experimental areas were located in Andalucia, in southern Spain, a region of Mediterranean climate characterized by warm and dry summers and cool and wet winters, with an average annual rainfall of over 550 mm. Two study sites were selected in the Cordoba and Seville provinces, respectively, to account for differences in weather conditions, crop age and tree-crown size, olive cultivars with different reactions to VW and VW incidence and severity. The first study site was located in Castro del Rio (Cordoba province, Spain) (37° 42′ 20″ N, 4° 30′ 45″ W) in a 7-ha commercial orchard planted in 2001 with the olive cultivar (cv.) Picual at a spacing of 6 × 4 m (Fig. 1a). Cv. Picual has been found to be highly susceptible to D and susceptible to ND *V. dahliae*, under controlled conditions in artificial inoculation tests (López-Escudero, del Rio, Caballero, & Blanco-López, 2004). The initial VW incidence (i.e., percentage of VW symptomatic trees) was estimated in 12%. The second study site was located in Utrera (Seville province, Spain) (37° 4′ 42″ N, 5° 50° 58″ W), in a 10-ha commercial orchard planted in 2006 with cv. Arbequina (Fig. 1b). Cv. Arbequina has been shown to be susceptible to D and moderately resistant to ND *V. dahliae*, under controlled conditions in artificial inoculation tests (López-Escudero et al., 2004). The olive trees were planted at a spacing of 6 × 3 m. The initial VW incidence was estimated in 30%. Both orchards were drip irrigated and managed using no-tillage practices; weed control was achieved with herbicide treatments between rows.

2.2. Verticillium wilt assessment

Incidence and severity of VW symptoms were assessed in both plots in spring and summer of 2009, 2010 and 2011 in coincidence with airborne campaigns. Severity of the disease was assessed by visual observation of foliar symptoms in each individual tree and assessment on a 0 to 4 rating scale according to the percentage of foliage with disease symptoms, where: 0 = 0%, 0.2 and 0.5 = initial symptoms, 1 = 1 to 33%, 2 = 34 to 66%, 3 = 67 to 100%, and 4 = dead plant. *V. dahliae* infection was confirmed in a sample from each experimental plot by isolating six stem fragments sampled from each of four young symptomatic branches per symptomatic tree as previously described (Navas-Cortés et al., 2008). Identification of *V. dahliae* isolates was based on the morphology of conidiophores and microsclerotia and confirmed by molecular typing through PCR assay using primers DB19/DB22/espdef01 (Mercado-Blanco, Rodríguez-Jurado, Parrilla-Araujo, & Jiménez-Díaz, 2003); this method yielded a polymorphic amplicon of 523 or 539 bp specific to *V. dahliae*. PCR amplification and gel electrophoresis were conducted as described previously (Mercado-Blanco et al., 2003).

2.3. Field measurements

Leaf and near-canopy field measurements were conducted in the olive orchard located in Castro del Rio (Cordoba) during the summer of 2011 to take: a) diurnal measurements throughout the day to monitor the diurnal variation of crown temperature (Tc − Ta) and stomatal conductance (G) in trees covering a gradient in severity levels; and b) leaf and crown measurements at midday to monitor the variation along the VW severity levels of Tc − Ta, leaf chlorophyll fluorescence, leaf Photochemical Reflectance Index (PRI_{570}) (Gamon et al., 1992) and leaf stomatal conductance (G). Eight trees showing different VW severity levels were selected to record pure crown temperature (Tc) with the objective of monitoring its diurnal variation. These measurements were conducted from 7:00 to 17:00 GMT at 5-minute intervals in two dataloggers (model CR10X, Campbell Sci., Logan, UT, USA) with infrared temperature (IRT) sensors (22° half-angle FOV) (model IRR-P, Apogee, Logan, UT, USA) placed 1 m above trees. The single-band infrared temperature (IRT) sensors covered the 6.5–14 μm range and were evaluated both in the laboratory and in field conditions to characterize the IRT response to diurnal temperature variation (Sepulcre-Cantó et al., 2006). The results yielded errors within the accuracy limits of the instrument (±0.4 °C) over a 5° to 40 °C range. The instruments were calibrated in the laboratory using a uniform calibration body (integrating sphere, CSTM-USS-2000C Uniform Source System, LabSphere, NH, USA) at two different levels of illumination. This procedure has been reported to be successful in other studies focused on monitoring crown temperature as an indicator of water stress (Berni, Zarco-Tejada, Suárez, & Fereres, 2009; Sepulcre-Cantó et al., 2006; Zarco-Tejada et al., 2012). Air temperature (Ta) and relative humidity (RH) were measured above the canopy with a portable weather station (Model WXT510, Vaisala, Finland) placed 1 m above the canopy (approx. 6 m above the ground). In each of the eight monitored trees, leaf stomatal conductance was measured from 7:00 to 17:00 GMT at 2-hour intervals with a leaf porometer (model SC-1, Decagon Devices, Washington, DC, USA) to monitor the diurnal variation of crown stomatal conductance for the different VW severity levels. A total of five illuminated leaves per tree were measured at each time interval.

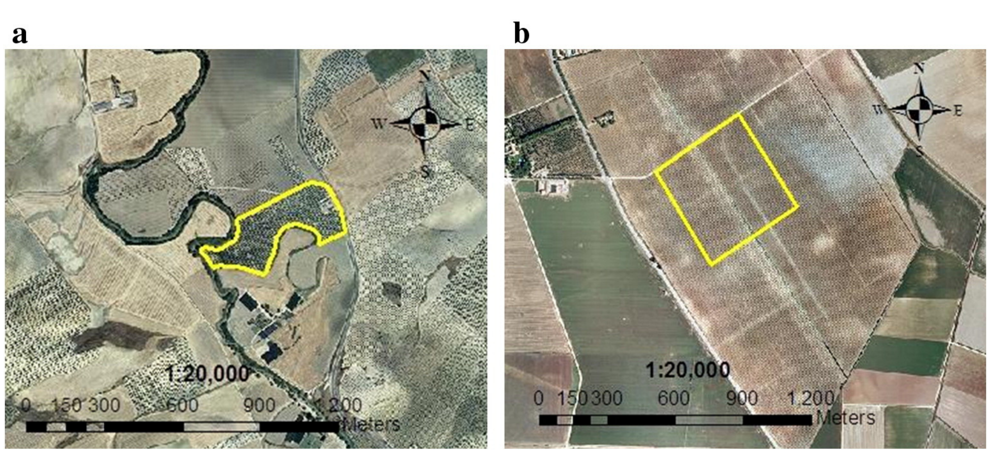

Fig. 1. Overview of the two study sites in southern Spain used in this study: (a) 7 ha commercial olive orchard in Castro del Rio (Cordoba province); and (b) 10-ha commercial olive orchard in Utrera (Seville province).

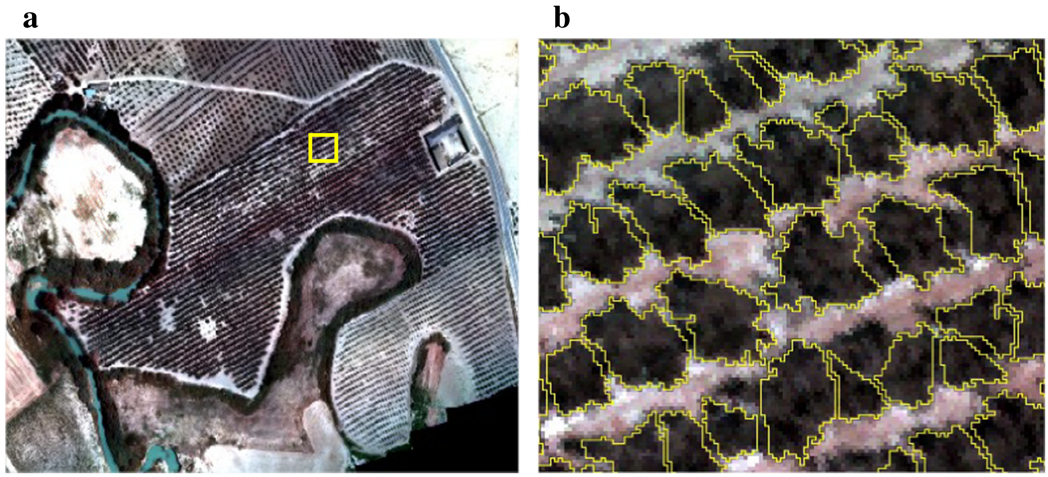

Fig. 2. Multispectral scene (a) obtained with the multispectral camera on board the UAV platform at 20-cm resolution, showing the Castro del Rio orchard study site (Córdoba province). (b) Automatic object-based crown detection applied to the multispectral imagery to identify pure olive crowns. Yellow square (a) shown in detail in (b). (For interpretation of the references to color in this figure legend, the reader is referred to the web version of this article.)

In addition to the diurnal measurements conducted for temperature and stomatal conductance, 25 trees covering a gradient in severity levels from asymptomatic to severely affected trees were chosen to monitor the variation of Tc − Ta, leaf chlorophyll fluorescence, leaf PRI_{570} and leaf G between 10:00 and 13:00 GMT on 27 and 28 July 2011. Leaf chlorophyll fluorescence measurements taken under natural sunlight

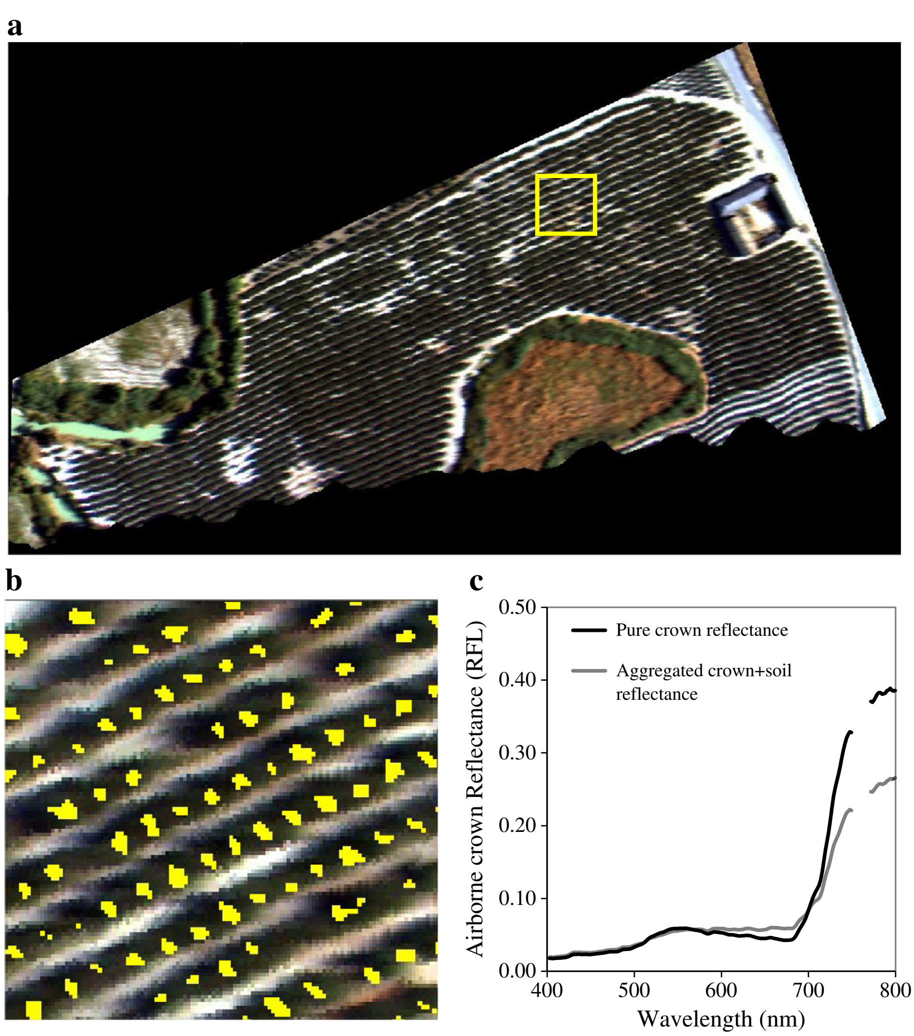

Fig. 3. Hyperspectral scene (a) obtained with the hyperspectral imager on board the UAV platform at 40 cm resolution. Automatic object-based crown detection applied to the hyperspectral imagery to identify pure olive crowns (b). The methodology enabled the separation of pure olive crowns from shaded and sunlit soil reflectance, observing the effects of pixel aggregation (c). Yellow square (a) shown in detail in (b). (For interpretation of the references to color in this figure legend, the reader is referred to the web version of this article.)

Table 1
Overview of the vegetation indices used in this study and their formulations.

Vegetation indices	Equation	Reference
Structural indices		
Normalized Difference Vegetation Index	$NDVI = (R_{800} - R_{670})/(R_{800} + R_{670})$	Rouse et al. (1974)
Renormalized Difference Vegetation Index	$RDVI = (R_{800}-R_{670})/\sqrt{(R_{800}+R_{670})}$	Rougean and Breon (1995)
Optimized Soil-Adjusted Vegetation Index	$OSAVI = ((1 + 0.16)\cdot(R_{800} - R_{670})/(R_{800} + R_{670} + 0.16))$	Rondeaux et al. (1996)
Triangular Vegetation Index	$TVI = 0.5\cdot[120\cdot(R_{750} - R_{550}) - 200\cdot(R_{670} - R_{550})]$	Broge and Leblanc (2000)
Modified Triangular Vegetation Index	$MTVI = 1.2\cdot[1.2\cdot(R_{800} - R_{550}) - 2.5\cdot(R_{670} - R_{550})]$	Haboudane et al. (2004)
Simple Ratio	$SR = R_{800}/R_{670}$	Jordan (1969)
Modified Simple Ratio	$MSR = \frac{R_{800}/R_{670}-1}{(R_{800}/R_{670})^{0.5}+1}$	Chen (1996)
Xanthophyll indices		
Photochemical Reflectance Index (570)	$PRI_{570} = (R_{570} - R_{531})/(R_{570} + R_{531})$	Gamon et al. (1992)
Photochemical Reflectance Index (515)	$PRI_{515} = (R_{515} - R_{531})/(R_{515} + R_{531})$	Hernández-Clemente et al. (2011)
Chlorophyll a+b indices		
RedEdge	$ZM = R_{750}/R_{710}$	Zarco-Tejada et al. (2001)
Vogelmann	$VOG1 = R_{740}/R_{720}$	Vogelmann et al. (1993)
Gitelson and Merzlyak indices	$GM1 = R_{750}/R_{550}$	Gitelson and Merzlyak (1997)
	$GM2 = R_{750}/R_{700}$	Gitelson and Merzlyak (1997)
Pigment Specific Simple Ratio Chlorophyll a	$PSSRa = R_{800}/R_{675}$	Blackburn (1998)
Pigment Specific Simple Ratio Chlorophyll b	$PSSRb = R_{800}/R_{650}$	Blackburn (1998)
Modified Chlorophyll-Absorption-Integral	$mCAI = \frac{(R_{545}+R_{752})}{2}\cdot(752-545)-\sum_{R_{545}}^{R_{752}}(R\cdot 1.158)$	Laudien et al. (2003)
Transformed Chlorophyll Absorption in Reflectance Index	$TCARI = 3\cdot[(R_{700} - R_{670}) - 0.2\cdot(R_{700} - R_{550})\cdot(R_{700}/R_{670})]$	Haboudane et al. (2002)
Transformed Chlorophyll Absorption in Reflectance Index/Optimized Soil-Adjusted Vegetation Index	$TCARI/OSAVI = \frac{3\cdot[(R_{700}-R_{670})-0.2\cdot(R_{700}-R_{550})\cdot(R_{700}/R_{670})]}{((1+0.16)\cdot(R_{800}-R_{670})/(R_{800}+R_{670}+0.16))}$	Haboudane et al. (2002)
R/G/B indices		
Redness index	$R = R_{700}/R_{670}$	Gitelson et al. (2000)
Greenness index	$G = R_{570}/R_{670}$	This study
Blue index	$B = R_{450}/R_{490}$	This study
Blue/green indices	$BGI1 = R_{400}/R_{550}$	Zarco-Tejada et al. (2005)
	$BGI2 = R_{450}/R_{550}$	Zarco-Tejada et al. (2005)
Blue/red indices	$BRI1 = R_{400}/R_{690}$	Zarco-Tejada et al. (2012)
	$BRI2 = R_{450}/R_{690}$	Zarco-Tejada et al. (2012)
Lichtenhaler index	$LIC3 = R_{440}/R_{740}$	Lichtenhaler et al. (1996)
Carotenoid indices		
Structure-Intensive Pigment Index	$SIPI = (R_{800} - R_{445})/(R_{800} + R_{680})$	Peñuelas et al. (1995)
Pigment Specific Simple Ratio Carotenoids	$PSSRc = R_{800}/R_{500}$	Blackburn (1998)
R_{520}/R_{500}	R_{520}/R_{500}	Zarco-Tejada et al. (2012)
R_{515}/R_{570}	R_{515}/R_{570}	Zarco-Tejada et al. (2012)
R_{515}/R_{670}	R_{515}/R_{670}	Zarco-Tejada et al. (2012)
Fluorescence		
FLD	$FLD3(747;762;780)$	Plascyk (1975) Maier et al. (2003) Zarco-Tejada et al. (2005)
Plant disease index		
Healthy-index	$HI = \frac{R_{534}-R_{698}}{R_{534}+R_{698}}-\frac{1}{2}\cdot R_{704}$	Mahlein et al. (2013)
Crop water stress index		
CWSI	$CWSI = \frac{\gamma\cdot(1+r_c/r_a)-\gamma^*}{\Delta+\gamma\cdot(1+r_c/r_a)}$	Jackson et al. (1981)

conditions were conducted using the PAM-2100 Pulse-Amplitude Modulated Fluorometer (Heinz Walz GMBH, Effeltrich, Germany). This device measured steady-state Fs and Fm' fluorescence parameters in 25 illuminated leaves per tree. Leaf PRI_{570} measurements calculated as $(R_{570} - R_{531}) / (R_{570} + R_{531})$ (Suárez et al., 2009, 2010, 2008; Zarco-Tejada et al., 2012) were taken in 25 illuminated leaves per tree with a PlantPen instrument custom designed to measure the R_{531} and R_{570} bands (Photon System Instrument, Brno, Czech Republic). Leaf G was measured in five illuminated leaves per tree with the leaf porometer previously used.

2.4. Airborne campaigns and remote sensing indices

Imagery in the three years of experiments was acquired from both study sites using narrow-band multispectral, hyperspectral and thermal cameras. The multispectral and thermal cameras were used in airborne campaigns conducted twice per crop season in spring (April/May) and summer (July) of 2009 and 2010. In addition, the thermal camera was flown twice in June 2011. The multispectral and thermal imagery was always acquired at similar sun angles at 10:30 and 12:00 GMT respectively to minimize differences due to sun angle effects between airborne campaigns. Hyperspectral and thermal images were acquired from the Castro del Rio site on 23 June 2011 at 9:00 GMT using a hyperspectral imager concurrently with the thermal camera operated in 2009 and 2010.

The flights were conducted with two different unmanned aerial vehicles (UAVs) operated by the Spanish Laboratory for Research Methods in Quantitative Remote Sensing (Quantalab, IAS-CSIC, Spain) (Berni, Zarco-Tejada, Suárez, & Fereres, 2009; Zarco-Tejada, Berni, Suárez, & Fereres, 2008, Zarco-Tejada et al., 2012). The UAV used for the multispectral and thermal acquisition had a 2-m wingspan for a fixed-wing platform at 5.8 kg take-off weight (TOW) (mX-SIGHT, UAV Services and Systems, Germany) capable of 1-hour endurance. Hyperspectral images were acquired with a larger UAV with a 5-m wingspan for a fixed-wing platform having 13.5 kg take-off weight (TOW) (Viewer, ELIMCO, Seville, Spain) capable of 3-hour endurance. This larger platform was required when operating the hyperspectral imager due to the heavier payload. Both UAV platforms were controlled

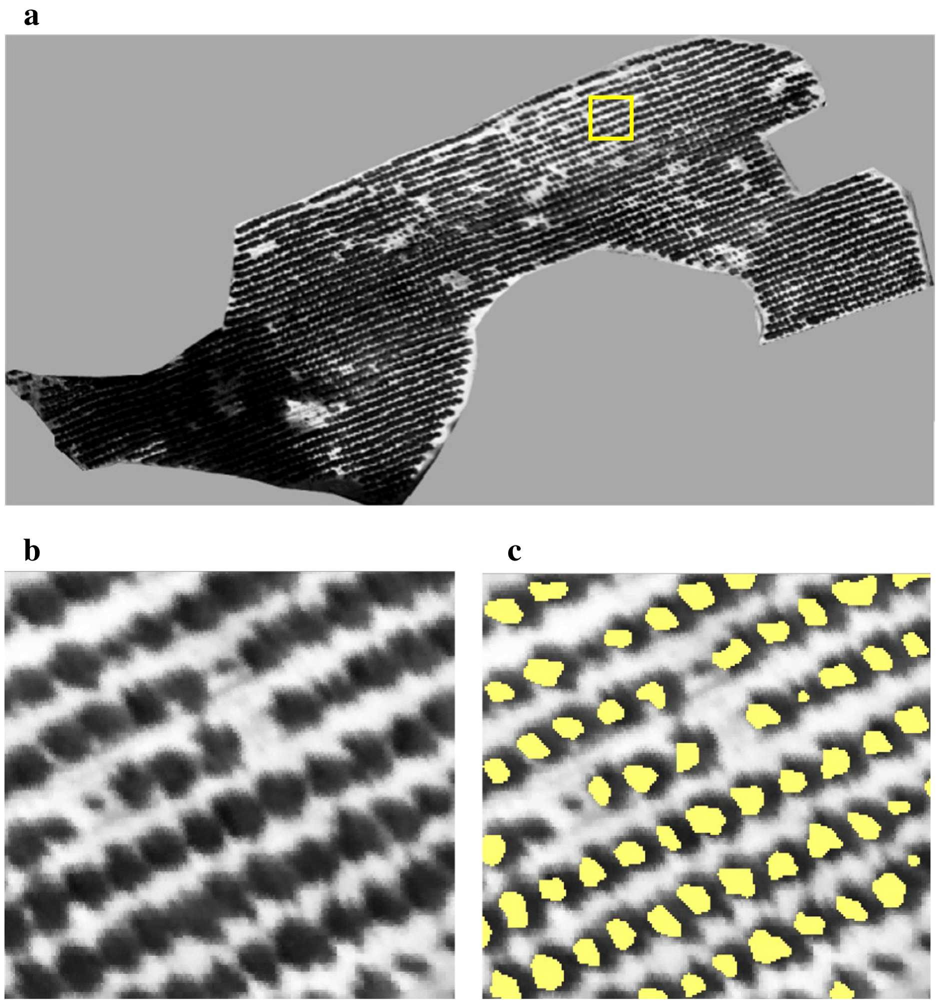

Fig. 4. Thermal scene (a) of the Castro del Rio site (Córdoba province) obtained with the thermal camera on board the UAV platform at 20-cm resolution, enabling pure olive crown identification (b). Automatic object-based crown detection applied to the thermal imagery to identify pure olive crowns (c). Yellow square (a) shown in detail in (b; c). (For interpretation of the references to color in this figure legend, the reader is referred to the web version of this article.)

by an autopilot system (AP04, UAV Navigation, Madrid, Spain) that provided autonomous navigation based on coordinates programmed during the mission planning.

Table 2
Inputs used to calculate the Crop Water Stress Index (CWSI) from high resolution airborne thermal imagery acquired in June 2011 in the Castro del Rio site. The CWSI was calculated as described in Berni et al. (2009a).

Inputs	Values	
	2 June 2011	15 June 2011
Air temperature (°C)	22.93	29.58
Relative humidity (%)	30.31	30.14
Wind speed (m/s)	1	1
Wind measurement height (m)	5	5
Atmospheric pressure (kPa)	99.45	99.60
Cloudiness	0.2	0.2
Latitude (°N)	37.7058	37.7058
Longitude (°E)	−4.5117	−4.5117
Altitude (m)	236	236
Solar time (decimal hour)	12.05	12.35
DOY	153	166
Canopy temperature (°C)	From image	From image
Canopy height (m)	4	4
Frontal LAI	1	1
Canopy emissivity ε	0.98	0.98

The multispectral sensor consisted of a 6-band multispectral camera (MCA-6, Tetracam, Inc., California, USA) flying at 250 m above ground level (AGL). The camera was equipped with six independent image sensors and optics with 25-mm diameter filters of 10-nm full width at half-maximum (FWHM) bandwidth (Berni, Zarco-Tejada, Suárez, & Fereres, 2009; Zarco-Tejada et al., 2009). Image resolution was 2592 × 1944 pixels with 10-bit radiometric resolution and an optical focal length of 8.4 mm, yielding an angular field of view (FOV) of 38.04° × 28.53° and a spatial resolution of 20 cm at 250 m altitude (Fig. 2a). The band sets used in each study site included centered wavelengths at 450, 490, 530, 570, 670 and 800 nm.

The hyperspectral imager (Micro-Hyperspec VNIR model, Headwall Photonics, MA, USA) was flown in 2011 at Castro del Río site in the spectral mode with 260 bands at 1.85 nm/pixel at 12-bit radiometric resolution. It yielded a 3.2-nm FWHM with a 12-micron slit and a 6.4-nm FWHM with a 25-micron slit. Data acquisition and storage on board the UAV was set to 50 fps with 18-ms integration time. The 8-mm optical focal length yielded an IFOV of 0.93 mrad and an angular FOV of 49.82°, obtaining a swath of 522 m at 53 × 42 cm resolution, resampled to 40 cm (Fig. 3a) for a flight conducted at 550 m AGL altitude and 75 km/h ground speed (Zarco-Tejada et al., 2012).

The multispectral and hyperspectral images were radiometrically calibrated with a uniform light source system (integrating sphere, CSTM-USS-2000C Uniform Source System, LabSphere, NH, USA) at four

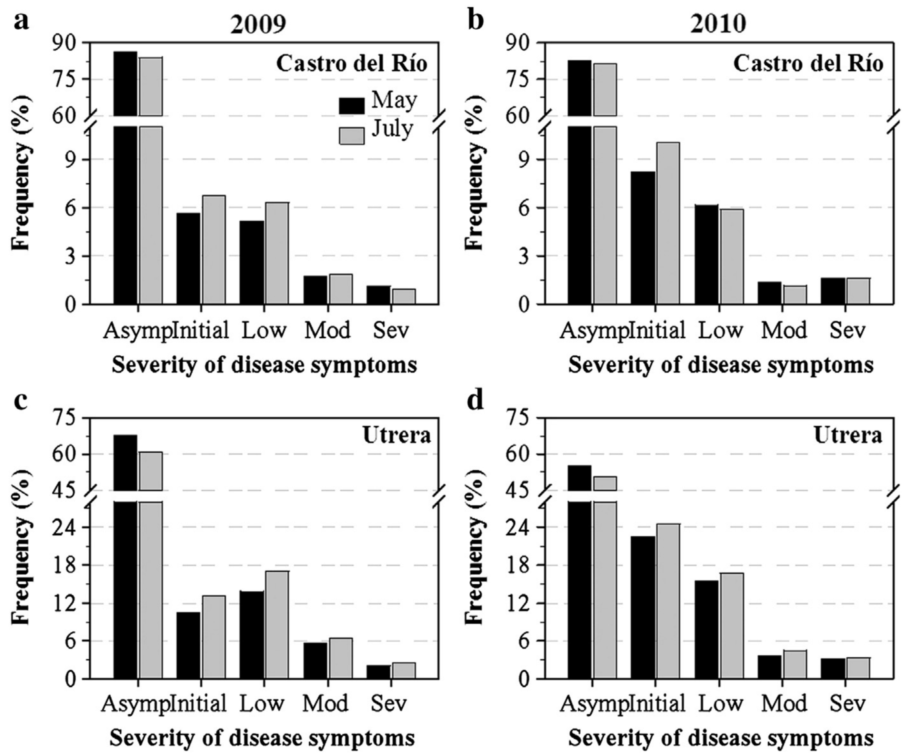

Fig. 5. Frequency (%) of olive trees showing *Verticillium* wilt (VW) symptoms at the different severity values in Castro del Rio (Córdoba province) (a,b) and Utrera (Seville province) (c,d) study sites assessed in May and July of 2009 (a,c) and 2010 (b,d). VW severity was assessed by visual inspection of each individual tree using a 0–4 rating scale according to percentage of foliage with disease symptoms, where: 0 = 0%, IS = initial symptoms, 1 = 1 to 33%, 2 = 34 to 66%, 3 = 67 to 100% and 4 = dead plant. Severity of disease symptoms was grouped in asymptomatic (DS = 0), initial (0.2 ≤ DS ≤ 0.5), low (1 ≤ DS ≤ 1.5), moderate (2 ≤ DS ≤ 2.5) and severe (3 ≤ DS ≤ 4) disease symptoms.

different levels of illumination and six different integration times. Atmospheric correction was performed with the SMARTS simulation model developed by the National Renewable Energy Laboratory, US Department of Energy (Gueymard, 1995, 2001). This was done using aerosol optical depth measured at 550 nm with a Micro-Tops II sunphotometer (Solar LIGHT Co., Philadelphia, PA, USA). This radiative transfer model has been used in previous studies to perform the atmospheric correction of both narrow-band multispectral and hyperspectral

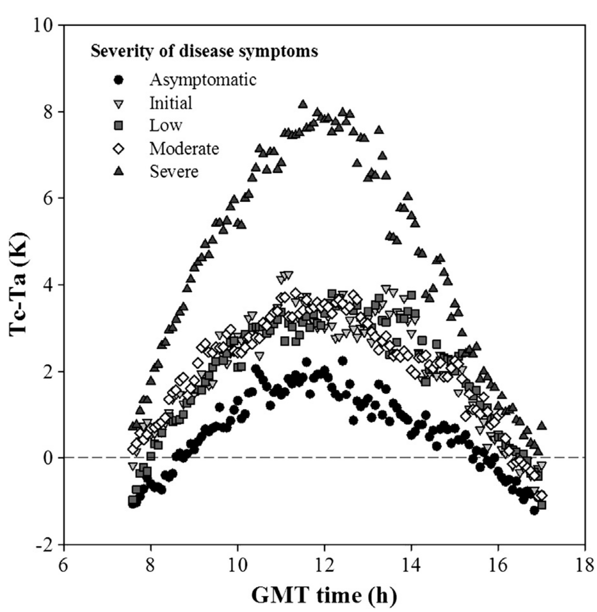

Fig. 6. Diurnal mean crown temperature (Tc − Ta) measured from 7:00 to 17:00 GMT at 5-minute intervals and obtained with the IRT sensors from trees showing different *Verticillium* wilt severity levels in the Castro del Rio site (Córdoba province) in the summer of 2011.

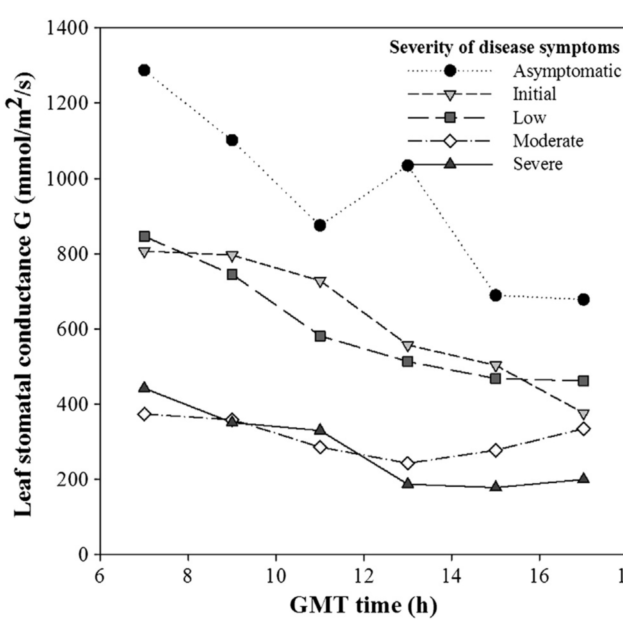

Fig. 7. Diurnal mean leaf stomatal conductance G measured from 7:00 to 17:00 GMT at 2-hour intervals and obtained with the leaf porometer from trees showing different *Verticillium* wilt severity levels (n = 5 per tree at each measuring time) in the Castro del Rio site (Córdoba province) in the summer of 2011.

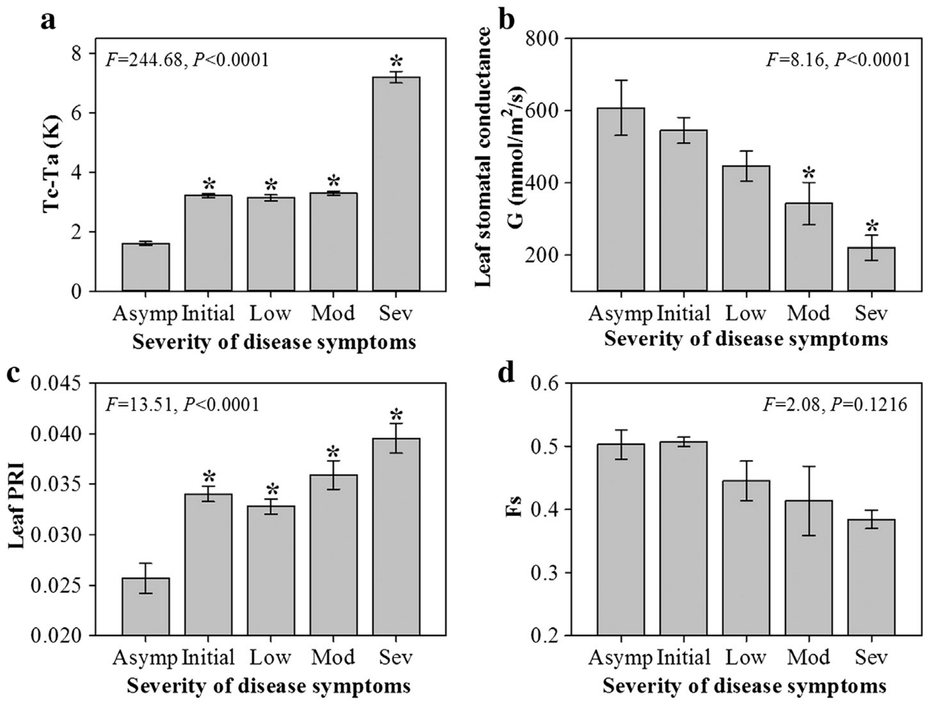

Fig. 8. Mean measurements of crown temperature (Tc − Ta) (a), leaf stomatal conductance (G) (b), leaf PRI_{570} (c) and leaf Fs (d) for every *Verticillium* wilt severity level. Analysis of variance of each index was conducted and asterisks indicate significant differences from the asymptomatic plants according to Dunnett's two-tailed test at $P < 0.05$. Error bars indicate standard errors.

imagery (Berni, Zarco-Tejada, Sepulcre-Cantó, Fereres, & Villalobos, 2009; Berni, Zarco-Tejada, Suárez, & Fereres, 2009; Suárez et al., 2010; Zarco-Tejada et al., 2012).

A miniaturized inertial measurement unit (IMU) installed on board the UAV and synchronized with the hyperspectral imager acquired altitude data at 100 Hz frequency. The imagery was later orthorectified using PARGE software (ReSe Applications Schläpfer, Wil, Switzerland) (Fig. 3a). The mean radiance and reflectance spectra calculated for the six spectral bands obtained by the multispectral camera and the 260 spectral bands acquired by the hyperspectral imager were then used to calculate several spectral indices related to: i) tree crown structure; ii) epoxidation state of the xanthophyll cycle; iii) chlorophyll a + b concentration; iv) blue/green/red ratio indices; v) carotenoid concentration; vi) chlorophyll fluorescence and vii) spectral disease indices (Table 1).

The chlorophyll fluorescence retrieval method used was based on the FLD principle (Plascyk, 1975) using three bands as in Maier et al. (2003) (see Zarco-Tejada et al., 2012 for fluorescence quantification in a citrus crop using this same hyperspectral imager). Previous results demonstrated the feasibility of retrieving the chlorophyll fluorescence signal using this hyperspectral imager (Zarco-Tejada, Catalina, González, & Martín, 2013, Zarco-Tejada et al., 2012). For this reason, the FLD principle could be applied to the hyperspectral imagery to estimate the fluorescence signal, using a total of three bands required for the FLD3 method, where the band inside the O_2-A feature (the "in" wavelength indicates the radiance at L763 nm) and the radiances (L750 nm; L780 nm) determined at two wavelengths outside and on either side of the O_2-A feature, referred to as the "out" bands.

The thermal camera (MIRICLE 307, Thermoteknix Systems Ltd, Cambridge, UK) installed on board the two UAVs operated in this study was flown over the experimental sites at altitudes ranging between 150 m and 250 m AGL in 2009 and 2010, and at 550 m AGL when flown together with the hyperspectral imager in 2011 in the morning (~9:00 GMT). This camera had a 14.25 mm f1.3 lens connected to a computer via a USB 2.0 protocol. The image sensor was a Focal Plane Array (FPA) based on uncooled microbolometers with a spectral range of 8–12 μm, yielding a 25 μm pixel size. The camera delivered raw images with a 640 × 480 pixel resolution and 14-bit at-sensor uncalibrated radiance. The camera was radiometrically calibrated in the laboratory using blackbodies at varying target and ambient temperatures to develop radiometric calibration algorithms along with an internal calibration for non-uniformity correction (NUC). Thermal images were acquired at 20 cm pixel resolution, enabling the retrieval of "pure crown" average temperature from each tree studied (Fig. 4a). Local atmospheric conditions were determined by air temperature, relative humidity and barometric pressure at the time of flight using a portable weather station (Model WXT510, Vaisala, Finland).

The high-resolution imagery acquired over the orchards enabled single tree identification for field validation purposes (Fig. 4b), successfully separating pure crown from soil pixels (Fig. 3c). Each single pure tree crown in the entire orchard was identified using automatic object-based crown detection algorithms (Figs. 2b;3b;4c). The algorithms applied to the thermal, multispectral and hyperspectral imagery enabled calculation of mean temperature and multispectral and hyperspectral reflectance at pure-crown level for the entire scenes acquired with the unmanned vehicles. The Crop Water Stress Index (CWSI) was calculated for each single tree crown using the high-resolution airborne thermal imagery acquired as described in Berni, Zarco-Tejada, Sepulcre-Cantó, Fereres, and Villalobos (2009), with the inputs detailed in Table 2.

2.5. Data analyses

Field and airborne data and indices calculated were subjected to standard analysis of variance (ANOVA) using the general linear model (GLM) procedure of SAS 9.2 (SAS Institute Inc., NC, USA). The Dunnett's two-tailed test was used to determine significant differences between asymptomatic trees and each of the disease severity levels at $P < 0.05$.

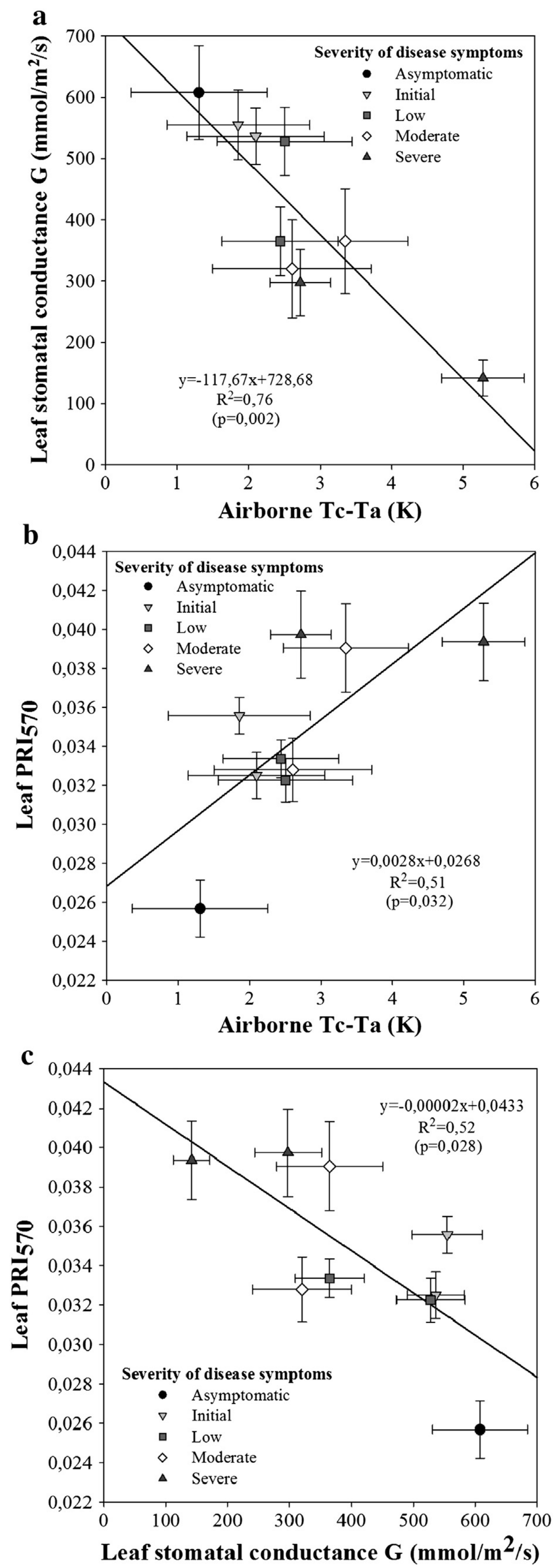

Fig. 9. Relationship between crown temperature extracted from the thermal imagery and leaf stomatal conductance (G) (a) and leaf PRI_{570} measurements (b) taken on olive trees showing different *Verticillium* wilt severity levels, and relationship between leaf G and leaf PRI_{570} (c). Thermal imagery was obtained at 11:00 GMT on 15 June 2011 and leaf measurements were obtained between 10:00 and 13:00 GMT on 27 and 28 July 2011 from crowns with different VW severity levels in the Castro del Rio study site (Córdoba province). Error bars indicate standard errors.

3. Results and discussion

3.1. Verticillium wilt symptom development

VW symptoms developed extensively in both study sites from early autumn to early winter, reaching their maximum expression during the spring. In the Utrera study site, characterized by 3-year-old cv. Arbequina olive trees, the symptoms consisted mainly of an extensive early drop of infected leaves that were still green; in most cases, this caused a complete defoliation and necrosis of affected branches. In the more established Castro del Rio study site, characterized by 10-yr old cv. Picual olive trees, affected plants mainly exhibited a quick dieback of olive twigs and branches where leaves turned light brown, rolled back toward the abaxial side and dried up, but typically remained attached to the symptomatic shoots. In both experimental sites, if the first VW symptoms developed in the spring, the trees underwent flower mummification and necrosis of both inflorescences and leaves of affected shoots, which usually fell. The type of VW symptoms and temporal dynamics of VW epidemics observed in both study sites were similar to those described in olive orchards affected by VW in southern Spain (Navas-Cortés et al., 2008).

In May 2009, 13.7 and 32.2% of trees were affected by VW in the Castro del Rio and Utrera study sites, respectively (Fig. 5a,c), with a mean disease severity in symptomatic trees of 1.26 and 1.19 (0–4 rating scale), respectively. These figures were determined from 41.4% that showed initial disease severity (DS) symptoms ($0 > DS \leq 0.5$), 37.5% had low disease severity symptoms ($0.5 > DS \leq 1.5$), 12.7% had moderate disease severity symptoms ($1.5 > DS \leq 2.5$) and 8.4% of symptomatic trees had severe ($DS \geq 3$) disease symptoms at Castro del Rio. At Utrera, 32.7, 43.0, 17.7 and 6.6% of trees showed these same severity levels, respectively (Fig. 5). During the spring of 2009, the disease progressed in both study sites to reach a global incidence of 15.9 and 39.3% in summer at Castro del Rio and Utrera, respectively (Fig. 5b,d); however, a similar frequency of trees remained in the three severity classes indicated above. In the 2010 season, overall disease incidence increased to 17.3 and 44.7% at Castro del Rio and Utrera, respectively (Fig. 5b,d), but mean disease severity decreased to 1.10 and 1.05 in both sites, respectively. However, minor differences were observed between both sites and the two assessment dates regarding the frequency of affected trees in the three severity classes. The overall frequency of trees at Castro del Rio in the four severity classes ranged from initial (47.3–53.9%), to low (35.6–31.4%), moderate (7.8–1.1%) and severe (9.3–1.6%) disease symptoms (Fig. 5b,d).

3.2. Field measurement results

Diurnal crown measurements were conducted with the IRT sensors on trees selected to represent asymptomatic trees and those showing initial, low, moderate and severe disease symptoms. Results revealed that midday (i.e., 10:00 to 14:00 GMT) was the best time period to maximize differences in $Tc - Ta$ values. In fact, $Tc - Ta$ values at midday increased with the rise in disease severity level (Fig. 6), showing up to 7 K temperature differences between asymptomatic trees ($DS = 0$) and severely affected trees ($DS \geq 3$). Moreover, $Tc - Ta$ values were able to discriminate asymptomatic trees from those affected at early stages of disease development ($DS \leq 1.5$), which showed $Tc - Ta$ values from 1 to 2.5 K higher. These results showing lower $Tc - Ta$ values in asymptomatic than in symptomatic diseased olive trees are in agreement with other studies. Thus, Nilsson (1995)

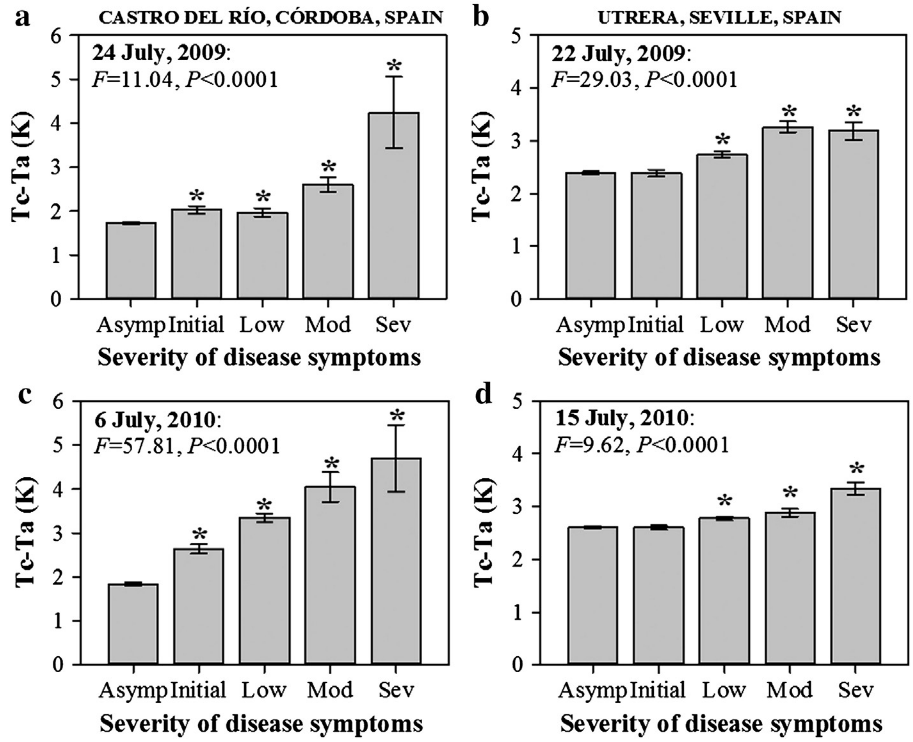

Fig. 10. Mean measurements of crown temperature (Tc − Ta) for every *Verticillium* wilt severity level. Tc − Ta was calculated from thermal imagery obtained in summer of two consecutive years (2009 and 2010) for the two study sites, Castro del Rio (Córdoba province) (a, c) and Utrera (Seville province) (b, d). Analysis of variance was conducted and asterisks indicate significant differences from the asymptomatic plants according to Dunnett's two-tailed test at $P < 0.05$. Error bars indicate standard errors.

reported higher leaf temperatures in oil seed plants infected with *V. dahliae*. The leaf stomatal conductance (G) data measured on the same trees consistently showed a decrease in stomatal conductance values as crown temperature and disease severity levels increased (Fig. 7). These results are in agreement with Berni, Zarco-Tejada, Suárez, and Fereres (2009) and Sepulcre-Cantó et al. (2006), who assessed the relationship between stomatal conductance and water stress levels due to deficit irrigation practices in olive trees using thermal sensors and a leaf porometer. A greater difference in stomatal conductance between healthy asymptomatic trees and VW-affected trees was recorded in the morning, with G differences up to 900 mmol/m^2/s between trees with extreme DS values (i.e., DS = 0 vs. DS ≥ 3). These differences decreased to a maximum of 700 mmol/m^2/s at midday and declined to 500 mmol/m^2/s after sunset. In addition, our results showed that stomatal conductance was able to discriminate between healthy trees and those at early stages of disease development, which had G values at least 300–500 mmol/m^2/s lower than those of healthy trees.

Data on crown temperature (Tc − Ta), leaf stomatal conductance (G), leaf PRI$_{570}$ and fluorescence (Fs) acquired between 10:00 and 13:00 GMT in July 2011 were analyzed in trees with different VW severity levels (Fig. 8). Crown temperature data (Tc − Ta) measured at midday with IRT sensors in VW affected trees was significantly ($P < 0.05$) higher than that measured in asymptomatic trees, being highest for trees affected by severe VW symptoms (Fig. 8a). By contrast, stomatal conductance G showed a negative trend as VW severity increased, showing significant ($P < 0.05$) changes from asymptomatic trees at those showing moderate and severe symptoms (DS ≥ 2) (Fig. 8b). Moreover, PRI$_{570}$ was lowest ($P < 0.05$) in asymptomatic trees, and increased steadily with the increase in VW severity (Fig. 8c). These results are consistent with that obtained by Suárez et al. (2008, 2009) in water-stressed trees. Leaf chlorophyll fluorescence measurements of Fs (Fig. 8d) showed a downward trend as VW severity level increased as previously found for trees under water stress (Pérez-Priego, Zarco-Tejada, Sepulcre-Cantó, Miller, & Fereres, 2005; Zarco-Tejada et al., 2009, 2012).

Leaf-level measurements conducted for temperature, stomatal conductance, fluorescence and the PRI$_{570}$ in healthy and VW symptomatic trees showed that Tc − Ta and PRI$_{570}$ were sensitive to *V. dahliae* infection and subsequent fungal colonization of affected trees and not simply influenced by structural effects driven by water stress. However, leaf G showed significantly lower values than asymptomatic trees in those affected by moderate or severe VW symptoms, while no significant differences in leaf Fs existed due to *V. dahliae* infection (Fig. 8).

3.3. Airborne hyperspectral, multispectral and thermal imagery results

3.3.1. Tree crown temperature (Tc − Ta) and CWSI

Crown temperature (Tc − Ta) extracted from the airborne thermal imagery in the summer of 2011 was compared against leaf stomatal conductance (G) and leaf PRI$_{570}$ data measured in 25 trees affected by VW (Fig. 9). Crown temperature (Tc − Ta) was significantly and linearly correlated with both the decrease of leaf G ($R^2 = 0.76$, $P = 0.002$; Fig. 9a) and the increase of PRI$_{570}$ ($R^2 = 0.51$, $P = 0.032$; Fig. 9b). Furthermore, leaf G showed an inverse linear correlation to the leaf PRI$_{570}$ ($R^2 = 0.52$, $P = 0.028$; Fig. 9c). Crown temperature (Tc − Ta) tended to increase as VW severity level increased (Fig. 10). VW affected trees showed up to 2 K higher Tc − Ta than that measured in healthy asymptomatic trees and were consistent in all measurements taken in April and July in both study sites. Indeed, symptomatic trees showed significantly ($P < 0.05$) higher Tc − Ta values than asymptomatic trees at any disease severity level at Castro del Rio, or at low or higher disease severity at Utrera. These results showed similar trends as those presented in Fig. 8a, with significant ($P < 0.05$) increases in Tc − Ta at leaf and canopy levels.

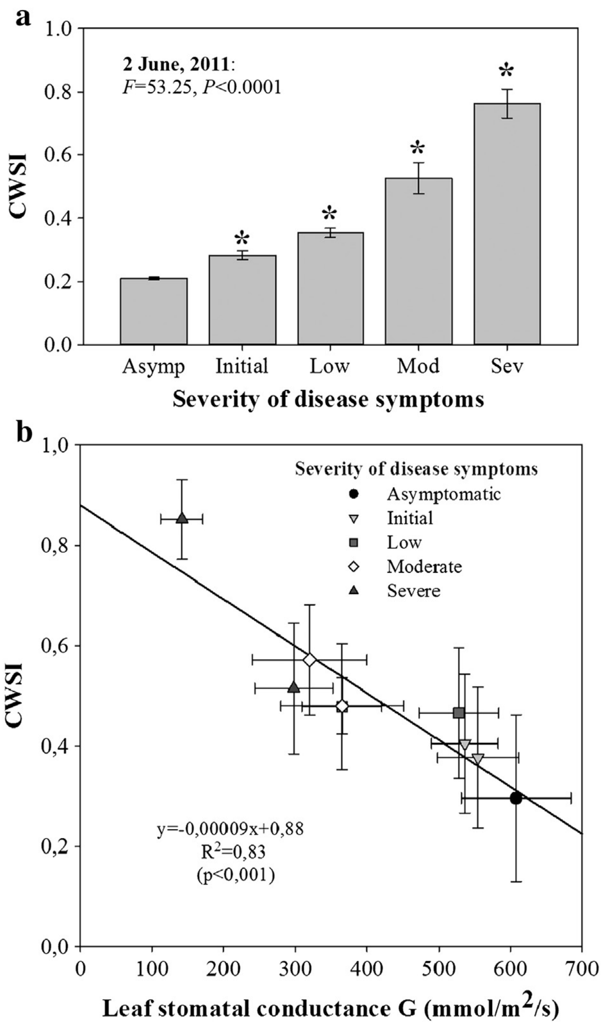

Fig. 11. (a) Mean values of Crop Water Stress Index (CWSI) for every *Verticillium* wilt severity level on 2 June 2011 in the Castro del Rio study site (Córdoba province). Analysis of variance was conducted and asterisks indicate significant differences from the asymptomatic plants according to Dunnett's two-tailed test at $P < 0.05$. Error bars indicate standard errors. (b) Relationship between leaf stomatal conductance (G) and the CWSI in trees with different VW severity levels. Leaf stomatal conductance measurements were obtained between 10:00 and 13:00 GMT on 27 and 28 July 2011 and the CWSI was calculated from the thermal imagery obtained at 11:00 GMT on 15 June 2011 in the Castro del Rio study site. Error bars indicate standard errors.

As expected, the CWSI estimated from the high-resolution airborne thermal imagery acquired on 2 June 2011 in the Castro del Rio site showed significantly ($P < 0.05$) lower values for asymptomatic trees, with an upward trend as VW severity level increased (Fig. 11a). CWSI derived from the thermal imagery on 15 June 2011 decreased linearly and significantly as a function of G obtained on 27 and 28 July 2011 ($R^2 = 0.83$; $P < 0.001$) (Fig. 11b). These results indicate that the CWSI obtained from high spatial resolution thermal imagery can be used to detect the lower transpiration rates induced by *V. dahliae* infection, as could be expected according to previous results (Berni, Zarco-Tejada, Sepulcre-Cantó, Fereres, & Villalobos, 2009) showing the usefulness of the CWSI as a water stress indicator. CWSI values estimated on the two different assessment dates in June 2011 were significantly ($P < 0.05$) lower for healthy trees than for those affected by the disease. At early stages of disease development (DS $\leq$ 1.5), CWSI ranged from 0.21 to 0.35 on 2 June 2011, and from 0.36 to 0.48 on 15 June 2011. At more advanced stages of VW development for trees affected by moderate or severe symptoms, CWSI values tended to increase, ranging from 0.35 to 0.76 on 2 June 2011 and from 0.48 to 0.71 on 15 June 2011.

3.3.2. Structural indices

The effects of VW on the canopy structure were captured by structural indices such as the NDVI (Fig. 12a), RDVI, OSAVI, TVI, MTVI, SR and MSR, that showed higher values for asymptomatic trees except for TVI and MTVI which showed an increase at early stages of disease development. Thus, moderate and severe VW wilt symptoms induced significantly ($P < 0.05$) lower values of NDVI, OSAVI, SR and MSR indices than those estimated in asymptomatic trees (Table 3). Furthermore, TVI and MTVI showed an increase ($P < 0.05$) in trees showing initial symptoms (Table 3). These results demonstrate the consistency of structural indices as VW damage indicator due to the expected effects on crown density at moderate or advanced stages of disease development.

3.3.3. Physiological indices

The revised xanthophyll indices were calculated based on PRI formulations using R_{570} as the reference band (PRI_{570}) (Fig. 12b) and the new formulation using band R_{515} as a reference to minimize structural canopy effects, PRI_{515} (Fig. 12c). These indices showed an upward trend as VW severity level increased. The PRI_{515} index was more sensitive to VW than PRI_{570}, and showed significantly ($P < 0.05$) lower values when trees were affected by moderate or severe symptoms (Table 3). This result confirms those obtained by Hernández-Clemente et al. (2011) in forest canopies and those of Stagakis, González-Dugo, Cid, Guillén-Climent, and Zarco-Tejada (2012) in orange and mandarin orchards, which demonstrated the robustness of the PRI_{515} to structural effects. Both, airborne-derived (Table 3) and leaf-level PRI_{570} (Fig. 8c) showed similar positive trend with disease severity, however only at leaf-level resulted in significant differences between healthy and VW affected trees. The chlorophyll indices TCARI (Fig. 12d) and TCARI/OSAVI showed an upward trend at early stages of the disease, reaching a maximum of 0.058 and 0.103 units at the low disease severity level, respectively, compared to 0.004 (TCARI) and 0.007 (TCARI/OSARI) observed for healthy trees. These results could indicate a decrease in chlorophyll a + b content (C_{a+b}) at early stages of *V. dahliae* infection (reducing stomatal conductance and photosynthesis rate). At advanced stages of the disease, the TCARI and TCARI/OSAVI inverted their trends due to the sharp leaf area index (LAI) drop associated with VW severity, showing significantly ($P < 0.05$) lower values at severe disease symptoms with 0.022 and 0.025 value drops between moderate and severely affected trees, respectively. The chlorophyll red edge index, VOG1, GM1, GM2, PSSRa and PSSRb showed significantly ($P < 0.05$) lower values on moderately and severely affected trees compared with values estimated on asymptomatic trees. The mCAI reached a significantly ($P < 0.05$) higher value at trees showing initial symptoms but steadily decreased in trees affected by moderate and severe symptoms.

The Greenness, red index and the blue/green ratio BG2 were not able to detect *V. dahliae* infection, since no significant ($P > 0.05$) changes were detectable when compared with healthy trees (Table 3). Interestingly, the blue index (Fig. 12e) could discriminate between healthy trees and those affected at any of the disease severity levels that reached significantly lower values ($P < 0.05$). Similarly, the blue/green ratio BG1 presented a significant ($P < 0.05$) decrease at early stages of disease development, but increased slightly at advanced stages, probably due to structural changes occurring in trees severely damaged by the pathogen. The blue/red ratios BR1 and BR2 showed downward trends with the increase in disease severity that resulted in significantly lower values at the initial, low and moderate symptom severity in BR1 (Fig. 12f) and low, moderate and severe in BR2. The LIC3 index showed a slightly decrease at early stages of the disease, followed by a significant ($P < 0.05$) increase on severely affected trees. The indices SIPI and PSSRc were inversely correlated with disease severity, showing significantly ($P < 0.05$) lower values at moderate and severe stages of disease development. The R_{520}/R_{500}, R_{515}/R_{570}, and R_{515}/R_{670} ratios were not useful for

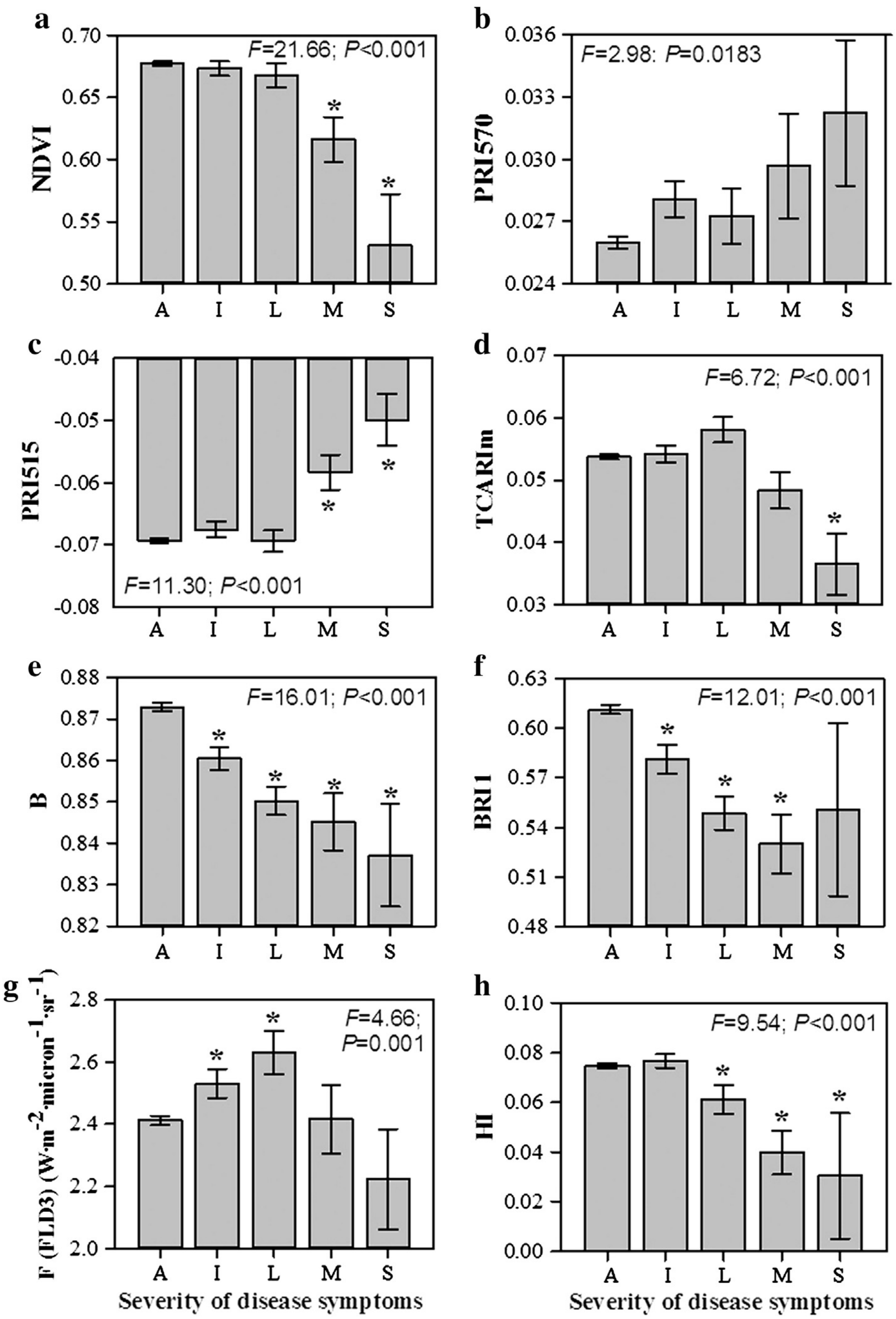

Fig. 12. Mean measurements of NDVI (a), PRI_{570} (b), PRI_{515} (c), TCARI (d), Blue index (B) (e), B/R index (BR1) (f), chlorophyll fluorescence FLD3 (g) and healthy-index (HI) (h) for every *Verticillium* wilt severity level. Analysis of variance of each index was conducted and asterisks indicate significant differences from the asymptomatic plants according to Dunnett's two-tailed test at $P < 0.05$. Error bars indicate standard errors.

the detection of VW as no significant differences were detected between asymptomatic and VW affected trees.

The chlorophyll fluorescence signal estimated from the hyperspectral imagery with the FLD method showed a significant ($P < 0.05$) increase at initial and low stages of disease symptom severity (2.677 $W \cdot m^{-2}\ \mu m^{-1} \cdot sr^{-1}$), slightly decreasing to 2.019 $W \cdot m^{-2} \cdot \mu m^{-1} \cdot sr^{-1}$ at the severe VW severity level (Fig. 12g). This result may indicate that the photosynthetic apparatus of the plant remains undamaged being able to dissipate the excess of energy by fluorescence that could not be maintained when the reduction in photosynthesis occurred at severely stressed plants, causing a decrease in the chlorophyll fluorescence rate. These results are in agreement with the studies conducted by Pérez-Priego et al. (2005) and Zarco-Tejada et al. (2009, 2012) in citrus and olive orchards under water stress conditions. Comparable results were obtained in airborne (Table 3) and leaf-derived chlorophyll fluorescence (Fig. 8d) that in both cases reached lower values in trees affected by moderate or severe symptoms. However, a significant ($P < 0.05$) increase in fluorescence occurred in trees at the early stage of disease development only at canopy level (Table 3). Finally, the health index (HI) developed to discriminate between healthy and diseased sugar beet leaves affected by

Table 3
Sensitivity of hyperspectral indices to *Verticillium* wilt symptoms in olive trees. Vegetation indices were calculated from the hyperspectral imagery obtained on 23 July 2011 in the Castro del Rio site (Córdoba province, Spain).

Vegetation indices	F[a]	P[a]	Severity of disease symptoms[b]			
			I	L	M	S
Structural indices						
NDVI	21.66	<0.001			X	X
RDVI	9.02	<0.001				X
OSAVI	11.52	<0.001			X	X
TVI	7.80	<0.001		X		X
MTVI	7.27	<0.001		X		X
SR	14.35	<0.001			X	X
MSR	16.49	<0.001			X	X
Xanthophyll indices						
PRI_{570}	2.98	0.0183				
PRI_{515}	11.30	<0.001			X	X
Chlorophyll a + b indices						
RedEdge	15.95	<0.001			X	X
VOG1	22.56	<0.001			X	X
GM1	10.99	<0.001			X	X
GM2	13.93	<0.001			X	X
PSSRa	14.70	<0.001			X	X
PSSRb	14.35	<0.001			X	X
mCAI	5.26	0.0003		X		
TCARI	6.72	<0.001				X
TCARI/OSAVI	3.30	0.0105				X
R/G/B indices						
R	12.27	<0.001				
G	16.51	<0.001				
B	16.01	<0.001	X	X	X	X
BG1	6.41	<0.001	X	X		
BG2	2.25	0.0611				
BR1	12.01	<0.001	X	X	X	
BR2	13.68	<0.001		X	X	X
LIC3	5.72	<0.001				X
Carotenoid indices						
SIPI	12.43	<0.001			X	X
PSSRc	9.73	<0.001			X	X
R_{520}/R_{500}	3.67	0.0055				
R_{515}/R_{570}	3.08	0.0152				
R_{515}/R_{670}	14.06	<0.001				
Fluorescence index						
FLD3	4.66	0.0010	X	X		
Plant disease indices						
HI	9.54	<0.001		X	X	X

[a] F statistic and P-value obtained from the standard analysis of variance (ANOVA).
[b] Significant changes in vegetation indices from asymptomatic plants according to Dunnett's two tailed test at $P < 0.05$ are indicated with X for initial (I) ($0.2 \leq DS \leq 0.5$), low (L) ($1 \leq DS \leq 1.5$), moderate (M) ($2 \leq DS \leq 2.5$) and severe (S) ($3 \leq DS \leq 4$) *Verticillium* wilt symptoms.

different foliar pathogens showed in this study lower values ($P < 0.05$) as the VW disease severity level increases to low, moderate or severe symptoms, respectively (Table 3; Fig. 12h).

4. Conclusions

The present study assessed remote sensing methods for early detection of *Verticillium* wilt in two olive orchards of different agronomic characteristics. It applied techniques based on the detection of the effects of *V. dahliae* infection and colonization on water flow that eventually cause water stress effects, assessed with thermal, multispectral and hyperspectral domains. It demonstrated that canopy temperature and physiological hyperspectral indices (i.e., PRI and chlorophyll fluorescence) are related with physiological stress caused by VW. Moreover, structural indices (i.e., NDVI) were more related to structural damage caused by VW. Field measurements showed large differences in temperature (Tc − Ta) and stomatal conductance (G) across VW severity levels, with higher Tc − Ta and lower G as severity level increased. This allowed identifying trees at the early stages of disease development. At leaf level, the reduction in transpiration and G caused by VW infection was associated with a significant ($P < 0.05$) increase in the PRI_{570} and a decrease in fluorescence. The flights conducted with thermal, multispectral and hyperspectral cameras enabled VW detection by using crown temperature (Tc − Ta; CWSI), assessing structural indices (NDVI, RDVI, OSAVI, TVI, MTVI, SR, MSR), the PRI_{515} index, chlorophyll indices (red edge, VOG1, GM1, GM2, PSSRa, PSSRb, mCAI, TCARI, TCARI/OSAVI), R/G/B indices (B, BG1, BR1, BR2, LIC3), carotenoid (SIPI and PSSRc), fluorescence, and the healthy index (HI). This study proved the potentials for the early detection of *V. dahliae* infection and discrimination among VW severity levels in olive crops using thermal, multispectral and hyperspectral imagery acquired with an unmanned aerial vehicle. Crown temperature, CWSI, B, BG1, BR1 and FLD3 were identified as the best indicators to detect VW at early stages of disease development, while NDVI, PRI_{515}, HI, and chlorophyll and carotenoid indices proved to be good indicators to detect the presence of moderate to severe damage.

Acknowledgments

Financial support from the Spanish Ministry of Education and Science for project AGL2009-13105 and from the Regional Government of Andalusia and the European Social Fund for project P08-AGR-03528 is gratefully acknowledged. R. Calderón is a recipient of research fellowship BES-2010-035511 from the Spanish Ministry of Education and Science. V. González-Dugo, J.A.J. Berni, D. Notario, A. Vera, A, Hornero, R. Romero and K. Gutierrez are acknowledged for their support during the field and airborne campaigns. M. Montes-Borrego, J.L. Trapero-Casas and G. León-Ropero are acknowledged for their technical support in *Verticillium* wilt assessments.

References

Ayres, P. G. (1978). Water relations of diseased plants. In T. T. Kozlowski (Ed.), *Water deficits and plant growth*, *Vol. 5*. (pp. 1–60)London, United Kingdom: Academic Press.
Barton, C. (2012). Advances in remote sensing of plant stress. *Plant and Soil*, *354*, 41–44.
Bauriegel, E., Giebel, A., Geyer, M., Schmidt, U., & Herppich, W. B. (2011). Early detection of *Fusarium* infection in wheat using hyper-spectral imaging. *Computers and Electronics in Agriculture*, *75*, 304–312.
Berni, J. A. J., Zarco-Tejada, P. J., Sepulcre-Cantó, G., Fereres, E., & Villalobos, F. J. (2009). Mapping canopy conductance and CWSI in olive orchards using high resolution thermal remote sensing imagery. *Remote Sensing of Environment*, *113*, 2380–2388.
Berni, J. A. J., Zarco-Tejada, P. J., Suárez, L., & Fereres, E. (2009). Thermal and narrow-band multispectral remote sensing for vegetation monitoring from an unmanned aerial vehicle. *IEEE Transactions on Geoscience and Remote Sensing*, *47*, 722–738.
Blackburn, G. A. (1998). Spectral indices for estimating photosynthetic pigment concentrations: A test using senescent tree leaves. *International Journal of Remote Sensing*, *19*(4), 657–675.
Blanco-López, M.A., Jiménez-Díaz, R. M., & Caballero, J. M. (1984). Symptomatology, incidence and distribution of *Verticillium* wilt of olive trees in Andalucia. *Phytopathologia Mediterranea*, *23*, 1–8.
Broge, N. H., & Leblanc, E. (2000). Comparing prediction power and stability of broadband and hyperspectral vegetation indices for estimation of green leaf area index and canopy chlorophyll density. *Remote Sensing of Environment*, *76*, 156–172.
Chen, J. (1996). Evaluation of vegetation indices and modified simple ratio for boreal applications. *Canadian Journal of Remote Sensing*, *22*, 229–242.
Chen, B., Li, S. K., Wang, K. R., Wang, J., Wang, F. Y., Xiao, C. H., et al. (2008). Spectrum characteristics of cotton canopy infected with *Verticillium* wilt and applications. *Agricultural Sciences in China*, *7*, 561–569.
Chen, B., Li, S., Wang, K., Zhou, G., & Bai, J. (2011). Evaluating the severity level of cotton *Verticillium* using spectral signature analysis. *International Journal of Remote Sensing*, *33*, 2706–2724.
Cohen, Y., Alchanatis, V., Meron, M., Saranga, Y., & Tsipris, J. (2005). Estimation of leaf potential by thermal imagery and spatial analysis. *Journal of Experimental Botany*, *56*, 1843–1852.
Dammer, K. H., Möller, B., Rodemann, B., & Heppner, D. (2011). Detection of head blight (*Fusarium* ssp.) in winter wheat by color and multispectral image analyses. *Crop Protection*, *30*, 420–428.
DeVay, J. E. (1989). Selection, characterization, pathogenicity and virulence of pectinase-deficient mutants of *Verticillium albo-atrum*. In E. C. Tjamos, & C. H. Beckman (Eds.), *Vascular wilt diseases of plants* (pp. 197–217). Berlin, Germany: Springer.
Dobrowsky, S. Z., Pushnik, J., Zarco-Tejada, P. J., & Ustin, S. L. (2005). Simple reflectance indices track heat and water stress induced changes in steady-state chlorophyll fluorescence at the canopy scale. *Remote Sensing of Environment*, *97*, 403–414.
Emechebe, A.M., Leaky, C. L. A., & Banage, W. B. (1975). *Verticillium* wilt of cacao in Uganda: Incidence and progress of infection in relation to time. *East African Agricultural and Forestry Journal*, *41*, 184–186.

Evain, S., Flexas, J., & Moya, I. (2004). A new instrument for passive remote sensing: 2. Measurement of leaf and canopy reflectance changes at 531 mm and their relationship with photosynthesis and chlorophyll fluorescence. *Remote Sensing of Environment*, *91*, 175–185.

Flexas, J., Briantais, J. M., Cerovic, Z., Medrano, H., & Moya, I. (2000). Steady-state and maximum chlorophyll fluorescence responses to water stress in grapevine leaves: A new remote sensing system. *Remote Sensing of Environment*, *73*, 282–297.

Flexas, J., Escalona, J. M., Evain, S., Gulias, J., Moya, I., Osmond, C. B., et al. (2002). Steady-state chlorophyll fluorescence (Fs) measurements as a tool to follow variations of net CO2 assimilation and stomatal conductance during water-stress in C-3 plants. *Physiologia Plantarum*, *114*(2), 231–240.

Flexas, J., Escalona, J. M., & Medrano, H. (1999). Water stress induces different levels of photosynthesis and electron transport rate regulation in grapevine. *Plant, Cell & Environment*, *22*, 39–48.

Gamon, J. A., Peñuelas, J., & Field, C. B. (1992). A narrow-wave band spectral index that tracks diurnal changes in photosynthetic efficiency. *Remote Sensing of Environment*, *41*, 35–44.

Garber, R. H., & Houston, B. R. (1966). Penetration and development of *Verticillium alboatrum* in the cotton plant. *Phytopathology*, *56*, 1121–1126.

Gitelson, A. A., & Merzlyak, M. N. (1997). Signature analysis of leaf reflectance spectra: Algorithm development for remote sensing of chlorophyll. *International Journal of Remote Sensing*, *18*, 2691–2697.

Gitelson, A. A., Yacobi, Y. Z., Schalles, J. F., Rundquist, D. C., Han, L., Stark, R., et al. (2000). Remote estimation of phytoplankton density in productive waters. *Archives in Hydrobiology — Special Issues in Advances in Limnology*, *55*, 121–136.

Gueymard, C. A. (1995). SMARTS, a simple model of the atmospheric radiative transfer of sunshine: Algorithms and performance assessment. *Technical report no. FSEC-PF-270-95*. Cocoa, FL: Florida Solar Energy Center.

Gueymard, C. A. (2001). Parameterized transmittance model for direct beam and circumsolar spectral irradiance. *Solar Energy*, *71*, 325–346.

Haboudane, D., Miller, J. R., Pattey, E., Zarco-Tejada, P. J., & Strachan, I. (2004). Hyperspectral vegetation indices and novel algorithms for predicting green LAI of crop canopies: Modeling and validation in the context of precision agriculture. *Remote Sensing of Environment*, *90*(3), 337–352.

Haboudane, D., Miller, J. R., Tremblay, N., Zarco-Tejada, P. J., & Dextraze, L. (2002). Integrated narrow-band vegetation indices for prediction of crop chlorophyll content for application to precision agriculture. *Remote Sensing of Environment*, *84*, 416–426.

Hatfield, P. L., & Pinter, P. J. (1993). Remote sensing for crop protection. *Crop Protection*, *12*, 403–413.

Hernández-Clemente, R., Navarro-Cerrillo, R. M., Suárez, L., Morales, F., & Zarco-Tejada, P. J. (2011). Assessing structural effects on PRI for stress detection in conifer forests. *Remote Sensing of Environment*, *115*, 2360–2375.

Hillnhütter, C., Mahlein, A. K., Sikora, R. A., & Oerke, E. C. (2011). Remote sensing to detect plant stress induced by *Heterodera schachtii* and *Rhizoctonia solani* in sugar beet fields. *Field Crops Research*, *122*, 70–77.

Idso, S. B., Jackson, R. D., Pinter, P. J., Reginato, R. J., & Hatfield, J. L. (1981). Normalizing the stress-degree-day parameter for environment variability. *Agricultural and Forest Meteorology*, *24*, 45–55.

Idso, S. B., Jackson, R. D., & Reginato, R. (1978). Extending the “degree day” concept of phenomenological development to include water stress effects. *Ecology*, *59*, 431–433.

Jackson, R. D. (1986). Remote sensing of biotic and abiotic plant stress. *Annual Review of Phytopathology*, *24*, 265–287.

Jackson, R. D., Idso, S. B., Reginato, R. J., & Ehrler, W. L. (1977). Crop temperature reveals stress. *Crop Soils*, *29*, 10–13.

Jackson, R. D., Idso, S. B., Reginato, R. J., & Pinter, P. J., Jr. (1981). Canopy temperature as a crop water stress indicator. *Water Resources Research*, *17*, 1133–1138.

Jackson, R. D., & Pinter, P. J., Jr. (1981). *Detection of water stress in wheat by measurement of reflected solar and emitted thermal IR radiation.* Spectral signatures of objects in remote sensing. Versalles, France: Institut National de la Reserche Agronomique, 399–406.

Jiménez-Díaz, R. M., Cirulli, M., Bubici, G., Jiménez-Gasco, L. M., Antoniou, P. P., & Tjamos, E. C. (2012). *Verticillium* wilt, a major threat to olive production: Current status and future prospects for its management. *Plant Disease*, *96*(3), 304–329.

Jiménez-Díaz, R. M., Olivares-García, C., Landa, B. B., Jiménez-Gasco, M. M., & Navas-Cortés, J. A. (2011). Region-wide analysis of genetic diversity in *Verticillium dahliae* populations infecting olive in southern Spain and agricultural factors influencing the distribution and prevalence of vegetative compatibility groups and pathotypes. *Phytopathology*, *101*, 304–315.

Jordan, C. F. (1969). Derivation of leaf area index from quality of light on the forest floor. *Ecology*, *50*, 663–666.

Krause, G. H., & Weis, E. (1984). Chlorophyll fluorescence as a tool in plant physiology. II. Interpretation of fluorescence signals. *Photosynthesis Research*, *5*, 139–157.

Laudien, R., Bareth, G., & Doluschitz, R. (2003). Analysis of hyperspectral field data for detection of sugar beet diseases. *Proceedings of the EFITA Conference, Debrecen, Hungary* (pp. 375–381).

Leinonen, I., & Jones, H. G. (2004). Combining thermal and visible imagery for stimulating canopy temperature and identifying plant stress. *Journal of Experimental Botany*, *55*, 1423–1431.

Levin, A. G., Lavee, S., & Tsror, L. (2003). Epidemiology of *Verticillium dahliae* on olive (cv. Picual) and its effects on yield under saline conditions. *Plant Pathology*, *52*, 212–218.

Lichtenhaler, H. K., Lang, M., Sowinska, M., Heisel, F., & Mieh, J. A. (1996). Detection of vegetation stress via a new high resolution fluorescence imaging system. *Journal of Plant Physiology*, *148*, 599–612.

López-Escudero, F. J., del Rio, C., Caballero, J. M., & Blanco-López, M.A. (2004). Evaluation of olive cultivars for resistance to *Verticillium dahliae*. *European Journal of Plant Pathology*, *110*, 79–85.

Mahlein, A. K., Rumpf, T., Welke, P., Dehne, H. W., Plümer, L., Steiner, U., et al. (2013). Development of spectral indices for detecting and identifying plant diseases. *Remote Sensing of Environment*, *128*, 21–30.

Maier, S. W., Günther, K. P., & Stellmes, M. (2003). Sun-induced fluorescence: A new tool for precision farming. In M. McDonald, J. Schepers, L. Tartly, T. van Toai, & D. Major (Eds.), *Digital imaging and spectral techniques: Applications to precision agriculture and crop physiology* (pp. 209–222). : ASA Special Publication.

Mengistu, A., Tachibana, H., Epstein, A. H., Bidne, K. G., & Hatfield, J.D. (1987). Use of leaf temperature to measure the effect of brown stem rot and soil moisture stress and its relation to yields of soybeans. *Plant Disease*, *71*, 632–634.

Mercado-Blanco, J., Rodríguez-Jurado, D., Parrilla-Araujo, S., & Jiménez-Díaz, R. M. (2003). Simultaneous detection of the defoliating and nondefoliating *Verticillium dahliae* pathotypes in infected olive plants by duplex, nested polymerase chain reaction. *Plant Disease*, *87*, 1487–1494.

Meroni, M., Colombo, R., & Cogliati, S. (November 17-19 2004). High resolution leaf spectral signature for the detection of solar induced chlorophyll fluorescence. *Proceedings of the 2nd ESA workshop on remote sensing of solar induced vegetation fluorescence. Montreal, Canada*.

Meroni, M., Picchi, V., Rossini, M., Cogliati, S., Panigada, C., Nali, C., et al. (2008). Leaf level early assessment of ozone injuries by passive fluorescence and PRI. *International Journal of Remote Sensing*, *29*(17–18), 5409–5422.

Meroni, M., Rossini, M., Guanter, L., Alonso, L., Rascher, U., & Colombo, R. (2009). Remote sensing of solar-induced chlorophyll fluorescence: Review of methods and applications. *Remote Sensing of Environment*, *113*, 2037–2051.

Meroni, M., Rossini, M., Picchi, V., Panigada, C., Cogliati, S., Nali, C., et al. (2008). Assessing steady-state fluorescence and PRI from hyperspectral proximal sensing as early indicators of plant stress: The case of ozone exposure. *Sensors*, *8*, 1740–1754.

Moya, I., Camenen, L., Evain, S., Goulas, Y., Cerovic, Z. G., & Latouche, G. (2004). A new instrument for passive remote sensing 1. *Measurements of sunlight-induced chlorophyll fluorescence. Remote Sensing of Environment*, *91*, 186–197.

Navas-Cortés, J. A., Landa, B. B., Mercado-Blanco, J., Trapero-Casas, J. L., Rodríguez-Jurado, D., & Jiménez-Díaz, R. M. (2008). Spatiotemporal analysis of spread of infections by *Verticillium dahliae* pathotypes within a high tree density olive orchard in southern Spain. *Phytopathology*, *98*, 167–180.

Nilsson, H. E. (1991). Hand-held radiometry and IR-thermography of plant diseases in field plot experiments. *International Journal of Remote Sensing*, *12*, 545–557.

Nilsson, H. E. (1995). Remote sensing and image analysis in plant pathology. *Annual Review of Phytopathology*, *15*, 489–527.

Papageorgiu, G. (1975). Chlorophyll fluorescence: An intrinsic probe of photosynthesis. In Govindjee (Ed.), *Bioenergetics of photosynthesis* (pp. 319–371). New York: Academic Press.

Peguero-Pina, J. J., Morales, F., Flexas, J., Gil-Pelegrín, E., & Moya, I. (2008). Photochemistry, remotely sensed physiological reflectance index and de-epoxidation state of the xanthophyll cycle in Quercus under intense drought. *Oecologia*, *156*(1), 1–11.

Peñuelas, J., Baret, F., & Filella, I. (1995). Semi-empirical indices to assess carotenoids/chlorophyll a ratio from leaf spectral reflectance. *Photosynthetica*, *31*, 221–230.

Pérez-Priego, O., Zarco-Tejada, P. J., Sepulcre-Cantó, G., Miller, J. R., & Fereres, E. (2005). Detection of water stress in orchard trees with a high-resolution spectrometer through chlorophyll fluorescence in-filling of the O2-A band. *IEEE Transactions on Geoscience and Remote Sensing*, *43*, 2860–2869.

Pinter, P. J., Stanghellini, M. E., Reginato, R. J., Idso, S. B., Jenkins, A.D., & Jackson, R. D. (1979). Remote detection of biological stresses in plants with infrared thermometry. *Science*, *205*, 585–587.

Plascyk, J. A. (1975). MK II Fraunhofer Line Dicsriminator (FLD-II) for airborne and orbital remote sensing of solar-stimulated luminescence. *Optical Engineering*, *14*(4), 339–346.

Presley, J. T., Carns, H. R., Taylor, E. E., & Schnathorst, W. C. (1966). Movement of conidia of *Verticillium albo-atrum* in cotton plants. *Phytopathology*, *56*, 375.

Raikes, C., & Burpee, L. L. (1998). Use of multispectral radiometry for assessment of *Rhizoctonia* blight in creeping bentgrass. *Phytopathology*, *88*, 446–449.

Reynolds, G. J., Windels, C. E., MacRae, I. V., & Laguette, S. (2012). Remote sensing for assessing *Rhizoctonia* crown and root rot severity in sugar beet. *Plant Disease*, *96*, 497–505.

Rondeaux, G., Steven, M., & Baret, F. (1996). Optimization of soil-adjusted vegetation indices. *Remote Sensing of Environment*, *55*, 95–107.

Rougean, J. -L., & Breon, F. M. (1995). Estimating PAR absorbed by vegetation from bidirectional reflectance measurements. *Remote Sensing of Environment*, *51*, 375–384.

Rouse, J. W., Haas, R. H., Schell, J. A., Deering, D. W., & Harlan, J. C. (1974). Monitoring the vernal advancement and retrogradation (green wave effect) of natural vegetation. *NASA/GSFC Type III Final Report, Greenbelt, Maryland* (pp. 371).

Sánchez-Hernández, M. E., Ruiz-Dávila, A., Pérez de Algaba, A., Blanco-López, M.A., & Trapero-Casas, A. (1998). Occurrence and etiology of death of young olive trees in southern Spain. *European Journal of Plant Pathology*, *104*, 347–357.

Sankaran, S., Mishra, A., Ehsani, R., & Davis, C. (2010). A review of advanced techniques for detecting plant diseases. *Computers and Electronics in Agriculture*, *72*, 1–13.

Schreiber, L. R., & Green, R. J., Jr. (1963). Effect of root exudates on germination of conidia and microsc1erotia of *Verticillium albo-atrum* inhibited by the soil fungistatic principle. *Phytopathology*, *53*, 260–264.

Sepulcre-Cantó, G., Zarco-Tejada, P. J., Jiménez-Muñoz, J. C., Sobrino, J. A., de Miguel, E., & Villalobos, F. J. (2006). Within-field thermal variability detection as function of water stress in *Olea europea* L. orchards with high resolution spatial remote sensing imagery. *Agricultural and Forest Meteorology*, *136*, 31–44.

Sepulcre-Cantó, G., Zarco-Tejada, P. J., Jiménez-Muñoz, J. C., Sobrino, J. A., Soriano, M.A., Fereres, E., et al. (2007). Monitoring yield and fruit quality parameters in open-canopy tree crops under water stress. Implications for ASTER. *Remote Sensing of Environment*, *107*, 455–470.

Sepulcre-Cantó, G., Zarco-Tejada, P. J., Sobrino, J. A., Berni, J. A. J., Jiménez-Muñoz, J. C., & Gastellu-Etchegorry, J. P. (2009). Discriminating irrigated and rainfed olive orchards with thermal ASTER imagery and DART 3D simulations. *Agricultural and Forest Meteorology*, *149*, 962–975.

Soukupová, J., Cséfalvay, L., Urban, O., Kosvancová, M., Marek, M., Rascher, U., et al. (2008). Annual variation of the steady-state chlorophyll fluorescence emission of evergreen plants in temperate zone. *Functional Plant Biology*, *35*, 63–76.

Stagakis, S., González-Dugo, V., Cid, P., Guillén-Climent, M. L., & Zarco-Tejada, P. J. (2012). Monitoring water stress and fruit quality in an orange orchard under regulated deficit irrigation using narrow-band structural and physiological remote sensing indices. *ISPRS Journal of Photogrammetry and Remote Sensing*, *71*, 47–61.

Suárez, L., Zarco-Tejada, P. J., Berni, J. A. J., González-Dugo, V., & Fereres, E. (2009). Modelling PRI for water stress detection using radiative transfer models. *Remote Sensing of Environment*, *113*, 730–740.

Suárez, L., Zarco-Tejada, P. J., González-Dugo, V., Berni, J. A. J., Sagardoy, R., Morales, F., et al. (2010). Detecting water stress effects on fruit quality in orchards with time-series PRI airborne imagery. *Remote Sensing of Environment*, *114*, 286–298.

Suárez, L., Zarco-Tejada, P. J., Sepulcre-Cantó, G., Pérez-Priego, O., Miller, J. R., Jiménez-Muñoz, J. C., et al. (2008). Assessing canopy PRI for water stress detection with diurnal airborne imagery. *Remote Sensing of Environment*, *112*, 560–575.

Sun, P., Grignetti, A., Liu, S., Casacchia, R., Salvatori, R., Pietrini, F., et al. (2008). Associated changes in physiological parameters and spectral reflectance indices in olive (*Olea europaea* L.) leaves in response to different levels of water stress. *International Journal of Remote Sensing*, *29*(6), 1725–1743.

Talboys, P. W. (1962). Systemic movement of some vascular pathogens. *Transactions of the British Mycological Society*, *45*, 280–281.

Thenot, F., Méthy, M., & Winkel, T. (2002). The photochemical reflectance index (PRI) as a water-stress index. *International Journal of Remote Sensing*, *23*(23), 5135–5139.

Tsror (Lahkim), L. (2011). Review: Epidemiology and control of *Verticillium* wilt on olive. *Israel Journal of Plant Sciences*, *59*, 59–69.

Tu, J. C., & Tan, C. S. (1985). Infrared thermometry for determination of root rot severity in bean. *Phytopathology*, *75*, 840–844.

Van Alfen, N. K. (1989). Reassessment of plant wilt toxins. *Annual Review of Phytopathology*, *27*, 533–550.

Vogelmann, J. E., Rock, B. N., & Moss, D.M. (1993). Red edge spectral measurements from sugar maple leaves. *International Journal of Remote Sensing*, *14*, 1563–1575.

Wang, D., Kurle, J. E., Estevez de Jensen, C., & Percich, J. A. (2004). Radiometric assessment of tillage and seed treatment effect on soybean root rot caused by *Fusarium* spp. in central Minnesota. *Plant and Soil*, *258*, 319–331.

West, J. S., Bravo, C., Oberti, R., Lemaire, D., Moshou, D., & McCartney, H. A. (2003). The potential of optical canopy measurement for targeted control of field crop diseases. *Annual Review of Phytopathology*, *41*, 593–614.

Winkel, T., Méthy, M., & Thénot, F. (2002). Radiation use efficiency, chlorophyll fluorescence, and reflectance indices associated with ontogenic changes in water-limited *Chenopodium quinoa* leaves. *Photosynthetica*, *40*(2), 227–232.

Zarco-Tejada, P. J., Berjón, A., López-Lozano, R., Miller, J. R., Marin, P., Cachorro, V., et al. (2005). Assessing vineyard condition with hyperspectral indices: Leaf and canopy reflectance simulation in a row-structured discontinuous canopy. *Remote Sensing of Environment*, *99*, 271–287.

Zarco-Tejada, P. J., Berni, J. A. J., Suárez, L., & Fereres, E. (2008). A new era in remote sensing of crops with unmanned robots. *SPIE Newsroom*, http://dx.doi.org/10.1117/2.1200812.1438.

Zarco-Tejada, P. J., Berni, J. A. J., Suárez, L., Sepulcre-Cantó, G., Morales, F., & Miller, J. R. (2009). Imaging chlorophyll fluorescence from an airborne narrow-band multispectral camera for vegetation stress detection. *Remote Sensing of Environment*, *113*, 1262–1275.

Zarco-Tejada, P. J., Catalina, A., González, M. R., & Martín, P. (2013). Relationships between net photosynthesis and steady-state chlorophyll fluorescence retrieved from airborne hyperspectral imagery. *Remote Sensing of Environment*, *136*, 247–258.

Zarco-Tejada, P. J., González-Dugo, V., & Berni, J. A. J. (2012). Fluorescence, temperature and narrow-band indices acquired from a UAV for water stress detection using a hyperspectral imager and a thermal camera. *Remote Sensing of Environment*, *117*, 322–337.

Zarco-Tejada, P. J., Miller, J. R., Mohammed, G. H., Notlamd, T. L. L., & Sampson, P. H. (2001). Scaling-up and model inversion methods with narrow-band optical indices for chlorophyll content estimation in closed forest canopies with hyperspectral data. *IEEE Transactions on Geoscience and Remote Sensing*, *39*, 1491–1507.